

**UNIVERSITY OF GAZİANTEP
GRADUATE SCHOOL OF
NATURAL & APPLIED SCIENCES**

**EFFECTS OF DIFFERENT MINERAL
ADMIXTURES ON THE SELF-HEALING
ABILITY OF ENGINEERED
CEMENTITIOUS COMPOSITES**

**M. Sc. THESIS
IN
CIVIL ENGINEERING**

**BY
GÜRKAN YILDIRIM
AUGUST 2012**

**Effects of Different Mineral Admixtures on the Self-
Healing Ability of Engineered Cementitious
Composites**

**M.Sc. Thesis
In
Civil Engineering
University of Gaziantep**

**Supervisor
Assoc. Prof. Dr. Mustafa ŞAHMARAN**

**by
Gürkan YILDIRIM
August 2012**

© 2012 [Gürkan YILDIRIM].

T.C.
UNIVERSITY OF GAZİANTEP
GRADUATE SCHOOL OF
NATURAL & APPLIED SCIENCES
CIVIL ENGINEERING DEPARTMENT


Name of the thesis: Effects of Different Mineral Admixtures on Self-Healing Ability
of Engineered Cementitious Composites

Name of the student: Gürkan YILDIRIM
Exam date: August 13, 2012

Approval of the Graduate School of Natural and Applied Sciences


Prof. Dr. Ramazan KOÇ
Director

I certify that this thesis satisfies all the requirements as a thesis for the degree of
Master of Science.


Prof. Dr. Mustafa GÜNAL
Head of Department

This is to certify that we have read this thesis and that in our opinion it is fully
adequate, in scope and quality, as a thesis for the degree of Master of Science.


Assoc. Prof. Dr. Mustafa ŞAHMARAN
Supervisor

Examining Committee Members

Signature

Assoc. Prof. Dr. Aytaç GÜVEN



Assist. Prof. Dr. Ömer PAYDAK



Assoc. Prof. Dr. Mustafa ŞAHMARAN



I hereby declare that all information in this document has been obtained and presented in accordance with academic rules and ethical conduct. I also declare that, as required by these rules and conduct, I have fully cited and referenced all material and results that are not original to this work.

Gürkan YILDIRIM

ABSTRACT

Effects of Different Mineral Admixtures on the Self-Healing Ability of Engineered Cementitious Composites

YILDIRIM, Gürkan

M.Sc. in Civil Engineering

Supervisor: Assoc. Prof. Dr. Mustafa ŞAHMARAN

August 2012, 70 pages

The presence of deleterious substances, such as chloride ion, and their transport are among the most important factors controlling the durability of cementitious composites, and the presence of mechanical loads on those causes cracks, which increases the permeability. The increase in permeability as a result of the cracks allows more chloride ions to penetrate into the cementitious composites, facilitating or speeding the deterioration. The present thesis studies the relationship among the applied mechanical deterioration in terms of splitting tensile deformation, curing conditions and chloride ion permeability of the Engineered Cementitious Composites (ECC) that contain different supplementary cementitious materials (SCMs). The splitting tensile deformations are introduced to generate microcracks in ECC specimens. After that, mechanically pre-cracked and pristine ECC specimens exposed to three different curing conditions (continuous wet, continuous air, and freeze-thaw cycle) up to two months. Rapid chloride permeability test (RCPT), microscopic observation and microstructural analysis were used to assess the rate and extent of self-healing. Test results indicate that the SCM type is very effective on the self-healing capacity of cementitious composites as measured by chloride ion permeability. Although ECC samples with fly ash have more unhydrated cementitious materials, and therefore, expectedly, a higher capacity for self-healing, more evident self-healing product was observed from ECC mixture incorporating slag indicating that the chemical productions stemming from SCM have great impacts on the self-healing capability of cementitious composites.

Keywords: Self-healing; Engineered Cementitious Composites (ECC); Supplementary cementitious material (SCM); Exposure conditions.

ÖZ

Farklı İlave Bağlayıcı Malzemeler İçeren Çimento Esaslı Kompozitlerin Kendiliğinden İyileşme Kapasitesinin Araştırılması

YILDIRIM, Gürkan
Yüksek Lisans Tezi, İnşaat Mühendisliği Bölümü
Tez Yöneticisi: Doç. Dr. Mustafa ŞAHMARAN
Ağustos 2012, 70 sayfa

Klorür iyonu gibi zararlı maddelerin varlığı ve taşınması, çimento esaslı kompozitlerde dayanıklılığı etkileyen en önemli faktörlerden biridir ve bu malzemeler üzerindeki mekanik yükler geçirimsizliği arttıran çatlaklara sebep olur. Çatlaklar sebebiyle artan geçirimsizlik bozulmayı kolaylaştıran ya da hızlandıran daha fazla klorür iyonunun kompozitlere geçişine olanak sağlar. Bu tezde, farklı ilave bağlayıcı malzemeler (İBM) içeren Tasarlanmış Çimento Esaslı Kompozitlerin (ECC) mekanik olarak hasara uğratılması, kür koşulları ve klorür iyonu geçirimsizliği arasındaki ilişki çalışılmıştır. Silindirik ECC numuneleri, mikroçatlaklar oluşturmak amacıyla yarmada çekme yüklemesi altında deformasyona uğratılmıştır. Daha sonra, hasarlı ve hasarsız ECC numuneleri iki ay boyunca üç farklı kür koşuluna maruz bırakılmıştır (sürekli su, sürekli hava ve donma-çözülme çevrimi). Kendiliğinden iyileşme sıklığının ve derecesinin değerlendirilmesi için hızlı klorür geçirimsizliği testi (HKGİT), mikroskopik gözlemler ve mikro yapı analizleri kullanılmıştır. Test sonuçları İBM çeşidinin ECC'nin kendiliğinden iyileşme kapasitesi üzerinde çok etkili olduğunu göstermektedir. UK-ECC numuneleri daha fazla reaksiyona girmemiş bağlayıcı malzeme miktarına ve bu sebeple kendiliğinden iyileşme için daha yüksek kapasiteye sahip olmalarına rağmen, cüruf ihtiva eden ECC numunelerinde kendiliğinden iyileşme ürünlerinin daha belirgin olduğu görülmüştür. Bu sonuç, İBM'lerden kaynaklanan kimyasal ürünlerin ECC numunelerinin kendiliğinden iyileşme kapasitesi üzerinde büyük etkileri olduğunu göstermektedir.

Anahtar Kelimeler: Tasarlanmış Çimento Esaslı Kompozitler (ECC); İlave bağlayıcı malzemeler; Kür koşulları.

ACKNOWLEDGEMENT

I am heartily thankful to my supervisor, Mustafa Sahmaran, whose encouragement, guidance and support from the initial to the final level enabled me to develop an understanding of the subject. This thesis would not have been possible without his support, inspiration, dedication of time and energy throughout the past year. I owe forever my deepest gratitude to him.

I must acknowledge the financial assistance of the Scientific and Technical Council of Turkey (TÜBİTAK) provided under Project: MAG-108M495.

Special thanks to Research Assistant Hasan Erhan YÜCEL and Hisham JASHAMI for their helps and invaluable suggestions.

I would also like to special thanks to Assist. Prof. Dr. Ömer PAYDAK and Assoc. Prof. Dr. Aytaç GÜVEN for serving on the committee.

Finally, I would like to thank my family members, especially my parents for supporting and encouraging me to pursue this degree. Without their encouragement, I would not have finished the degree.

TABLE OF CONTENTS

	Page
ABSTRACT	V
ÖZ.....	VI
ACKNOWLEDGEMENT	VII
TABLE OF CONTENTS.....	VIII
LIST OF FIGURES	XI
LIST OF TABLES	XIV
LIST OF SYMBOLS/ABBREVIATIONS.....	XV
INTRODUCTION.....	1
1.1 General	1
1.2 Research Objectives and Scope	3
CHAPTER II.....	5
LITERATURE REVIEW AND BACKGROUND.....	5
2.1 Introduction.....	5
2.2 Engineered Cementitious Composites (ECC).....	6
2.3 Design of Engineered Cementitious Composites.....	8
2.4 Self Healing in ECC.....	10
2.4.1 Conditions for Reliable Self-Healing.....	10
2.4.2 Effect of Crack Width on Self-Healing.....	11

2.4.3 Self-Healing Mechanism.....	13
2.4.4 Self-Healing Examination Methods.....	14
2.4.4.1 Dynamic Modulus Measurements	14
2.4.4.2 Uniaxial Tensile Test	16
2.4.4.3 Water Permeability Test (WPT)	19
2.4.4.4 Rapid Chloride Permeability Test (RCPT).....	22
2.4.4.5 Microscopic Observation and Analysis	24
2.5 Pozzolanic Material.....	25
2.5.1 Slag.....	25
2.5.2 Fly Ash.....	27
CHAPTER III	28
EXPERIMENTAL PROGRAM.....	28
3.1 Materials.....	28
3.1.1 Portland Cement.....	28
3.1.2 Mineral Admixtures	29
3.1.2.1 Class-F Fly Ash.....	29
3.1.2.2 Class-C Fly Ash	30
3.1.2.3 Slag	30
3.1.3 Aggregate	30
3.1.4 Chemical Admixtures	31
3.1.5 Polyvinyl Alcohol (PVA) Fiber	31
3.2 ECC Mixing and Specimen Preparation	32
3.3 Pre-cracking and Self-Healing Evaluation Methods.....	35

3.4 Environmental Conditioning.....	37
3.5 Test Procedure.....	37
3.5.1 Compressive Strength	37
3.5.2 Flexural Performance.....	38
3.5.3 Freezing and Thawing Test.....	39
3.5.4 Rapid Chloride Permeability Test (RCPT)	40
CHAPTER IV.....	41
RESULTS AND DISCUSSIONS	41
4.1 Compressive Strength	41
4.2 Flexural Performance.....	42
4.2.1 Flexural Strength (modulus of rupture – MOR)	42
4.2.2 Mid-span Beam Deflection	43
4.3 Rapid Chloride Permeability Test.....	44
4.3.1 Unhealed Specimens	44
4.3.2 Effects of Self-Healing.....	50
4.4 Crack Characteristics and Microstructure.....	55
CHAPTER V	61
CONCLUSIONS	61
REFERENCES.....	63

LIST OF FIGURES

	Page
Figure 2.1 Typical tensile stress-strain curve and crack width development of ECC (Weimann and Li, 2003)	7
Figure 2.2 Response of ECC under flexural loading	8
Figure 2.3 Crack bridging stress versus crack opening relation	9
Figure 2.4 Resonant frequency (RF) ratio as a function of crack width (Yang et al., 2009)	12
Figure 2.5 Permeability coefficient as a function of crack width before and after conditioning (Yang et al., 2009)	12
Figure 2.6 Self-healing rate of ECC under cyclic wetting and drying: (a) Resonant frequency recovery under CR1 (water/air cycle); (b) Resonant frequency recovery under CR2 (water/hot air cycle) (Li and Yang, 2007)	15
Figure 2.7 Extent of self-healing in ECC under cyclic wetting and drying: (a) Extent of self-healing in ECC under CR1 (water/air cycle); (b) Extent of self-healing in ECC under CR2 (water/hot air cycle) (Li and Yang, 2007)....	15
Figure 2.8 Uniaxial tensile test set up	17
Figure 2.9 Preloading and reloading after 10 CR1 (water/air) cycles tensile stress–strain relations of ECC specimens: (a) Specimen with preloading above 1%; (b) Specimen with preloading to or below 1%, Preloading and reloading after 10 CR2 (water/hot air) cycles tensile stress–strain relations of ECC specimens: (c) Specimen with preloading above 1%; (d) Specimen with preloading to or below (Li and Yang, 2007).....	18

Figure 2.10 (a) Preloading and reloading without self healing tensile stress–strain curve of ECC specimens, (b) Stiffness recovery of ECC under different conditioning regime (Li and Yang, 2007).....	19
Figure 2.11 (a) Falling Head Permeability Test Setup (Cernica, 1982) (b) Constant Head Permeability Test Setup (Wang et al., 1997).....	20
Figure 2.12 Development of Permeability for ECC Strained to 1.5%, 2%, and 3% (Lepech and Li, 2009).....	21
Figure 2.13 Appearance of ECC permeability specimens: (a) before permeability testing and (b) after permeability testing (Lepech and Li, 2009).....	22
Figure 2.14 Chloride ion permeability values of the ECC mixtures under different curing conditions and testing ages Ozbay et al. (2011)	23
Figure 2.15 SEM micrograph with EDX pattern of rehydration products in a self-healed crack (ECC-2, after 60 days moist curing) Ozbay et al. (2011) ...	24
Figure 3.1 Particle size distributions of sand, portland cement and SCMs.....	29
Figure 3.2 Particle morphology of a) Class-F fly ash b) Class-C fly ash c) slag determined by SEM.....	29
Figure 3.3 PVA Fiber used in the production of ECC	31
Figure 3.4 Production of ECC by using Hobart Type mixer	33
Figure 3.5 Curing of ECC specimens after production of them (a) Cube and prism specimens, (b) Cylindrical specimens.....	34
Figure 3.6 Splitting tensile strength test setup	35
Figure 3.7 Control of crack widths of specimens tested by splitting tensile test.....	36
Figure 3.8 Compression testing machine and cubic samples.....	38
Figure 3.9 Four-point bending test setup	38
Figure 3.10 Four-point flexural strength test	39

Figure 3.11 Specimens in freezing and thawing machine.....	40
Figure 3.12 Rapid chloride permeability test (RCPT) setup.....	40
Figure 4.1 SEM image from the fractured surface.....	43
Figure 4.2 Changes in pore size distribution of ECC mixtures	46
Figure 4.3 SEM observations of F_ECC mixture at 60 days of age.....	47
Figure 4.4 Chloride ion permeability values of the ECC mixtures under different curing conditions and testing ages	49
Figure 4.5 Percent variations in chloride ion permeability values of ECC mixtures due to the curing regimes and testing ages.....	52
Figure 4.6 Surface conditions of ECC specimens after 300 F/T cycles.....	54
Figure 4.7 Self-healing in ECC microcracks before and after exposure to CW curing	56
Figure 4.8 SEM micrograph with EDX pattern of products in self-healed cracks	58
Figure 4.9 XRD patterns of self-healing products in ECC mixtures	59

LIST OF TABLES

	Page
Table 2.1 Typical mix design of ECC material.....	6
Table 2.2 Specifications for fly ash (ASTM C 618, 2003).....	27
Table 3.1 Chemical properties of Portland cement, fly ashes and slag.....	28
Table 3.2 Mechanic and Geometric Properties of PVA Fibers.....	32
Table 3.3 ECC mixture proportions containing fly ash and slag, by weight	32
Table 4.1 Basic mechanical properties of ECC mixtures	42
Table 4.2 Rapid chloride permeability test results of ECC specimens.....	45

LIST OF SYMBOLS/ABBREVIATIONS

C	Class-C fly ash
CA	Continuous air
CH	Calcium hydroxide
C-S-H	Calcium-silicate-hydrate
CW	Continuous wet
ECC	Engineered cementitious composites
EDX	Energy dispersive X-ray analysis
F	Class-F fly ash
FA	Fly ash
FRC	Fiber reinforced concrete
F/T	Freeze/thaw cycle
HPFRCC	High performance fiber reinforced cementitious composites
HVFA	High volume fly ash
LVDT	Linear variable displacement transducer
MA/PC	Mineral admixture to Portland cement ratio
MIP	Mercury intrusion porosimetry
MOR	Modulus of rupture
PC	Portland cement

PVA	Polyvinyl-alcohol fibers
RCPT	Rapid chloride permeability test
R/C	Reinforced concrete
RH	Relative humidity
S	Ground granulated blast furnace slag
SCM	Supplementary cementitious materials
SEM	Scanning electron microscopy
W/CM	Water to cementitious material ratio
XRD	X-ray diffraction
XEDS	X-Ray Energy Dispersive Spectroscopy

INTRODUCTION

1.1 General

Lack of durability has recognized a major concern in construction practices for the past decades. In order for safety requirements to be fulfilled, it is vital to know whether durability needs are ensured or not. In the cases where durability of a concrete material is of interest, cracking which can cause keen decreases in durability properties must be taken into account. Concrete may crack throughout the service life of a structure. The cracks may originate from external effects, harsh environment, poor workmanship or due to concrete itself in the case of restraining conditions. Cracks affect concrete structures in a manner that they lose their durability and serviceability properties in time. The presence of cracks decrease the load carrying capacity, influence the mechanical properties such as compressive strength and elastic modulus and allows for aggressive ions to penetrate into concrete itself and reinforcing bars by creating additional pathways, which can lead to further cracking and disintegration in time (Mehta and Gerwick,1982). Since, the low durability of concrete structures can be associated with the brittle nature of concrete, improvement of new class of concretes that can compensate the lack of performance is extremely desirable. Along these lines, a new type of composite called Engineered Cementitious Composites (ECC) has been developed in last decades.

ECC is a special type of high performance fiber-reinforced cementitious composite (HPFRC) featuring high ductility and damage tolerance under mechanical loading, including tensile and shear loadings (Li, 1998; Li, 2003). By employing micromechanics-based material optimization, tensile strain capacity in excess of 3% under uniaxial tensile loading can be attained with only 2% fiber content, by volume (Li, 1998; Lin and Li, 1997; Lin et al., 1999). Strain-hardening behavior which is one of the material characteristics of ECC is associated with the multiple tight crack phenomenon of the brittle matrix. Multiple tight crack width with the width of

generally less than 100 μm , which is self-controlled and free of reinforcement is an intrinsic characteristic of ECC. The tight crack width is a significant parameter in realizing the relation correlated to self-healing. Self-healing ability of cracked concrete is a frequently studied phenomenon. Experimental research and practical experience have demonstrated that cracks in concrete material itself have potential to seal themselves. Self-healing is generally attributed to the hydration of previously unhydrated cementitious material, calcite formation, expansion of the concrete in the crack flanks, crystallization, closing of cracks by solid matter in the water and closing of the cracks by spalling of loose concrete particles resulting from cracking (Jacobsen et al., 1995). Self-healing of cracks should be taken into account when specifying tolerable crack widths. Jacobsen et al. (1995), Reinhardt and Jooss (2003), Edvardsen (1999), Aldea et al. (2000) and Clear (1985) have proposed the maximum crack widths as 5 to 10 μm , 100 μm , 200 μm , 205 μm and 300 μm , respectively in order for a crack to seal itself completely. In all, it is pointed out that the most serious challenge for complete healing of a crack is tolerable crack width. Because conventional concrete has the tendency to deform in a brittle manner under mechanical loading, such small crack widths could be a major concern to attain. Since the crack width was identified as a key factor in the self-healing of concrete materials, tight crack widths in ECC are likely to promote self-healing behavior.

Lately, there are increasing concerns related to raw material depletion, global warming and climate change with the exponential growth of human population and industrialization. However, the environmental aspects of portland cement are a growing concern, as cement manufacturing is responsible for about 7% of total worldwide emissions from industrial sources. One effective way to reduce the environmental impact is to use supplementary cementitious materials (SCM), as a partial cement replacement. This strategy will have the potential to reduce costs, conserve energy, and reduce waste volumes. Supplementary cementitious materials (SCMs) are silica-based materials that react to form hydration products when introduced in portland cement paste, so they can partially replace portland cement. Recently, usage of SCMs as a component of ECC has become usual (Şahmaran and Li, 2007; Wang and Li, 2007; Qian et al., 2009). SCMs are used for several reasons through the production of ECC. The absence of coarse aggregates in ECC results in higher portland cement content. Therefore, partial replacement of portland cement

with SCMs can lower the material cost, reduce environmental burden and enhance its greenness, since the production of these materials needs less energy and causes less carbon dioxide emission than cement. Among the various supplementary materials, fly ash and ground granulated blast furnace slag are the most commonly available SCMs. These by-products are available in large quantities, and compared to cement, they are generally cheaper and greener.

While knowledge of the effect of SCMs on the mechanical and durability properties of cementitious composites is available, the effects of SCM types on self-healing capability of ECC are very limited in literature, especially in the case of exposure to various environmental conditions and pre-loading deformation levels. In the present work, it was aimed to create an understanding on the influences of different mineral admixture types on the structures in different environmental exposures in order to simulate outdoor environmental conditions in which ECC structures are exposed. For this purpose, ECC mixtures, which contain different mineral admixture types, were produced and exposed to the different splitting tensile pre-loading deformation levels for the disturbance of specimens. Three typical SCMs (i.e., a low-calcium fly ash, a high-calcium fly ash and a slag) were used, representing a wide range of chemical compositions, from highly pozzolanic to almost cementitious. The pre-applied deformation can be a combination of strain due to vehicle load, prestressing load, shrinkage, thermal load, etc. The specimens were then exposed to three different outdoor environmental conditions (continuous air (CA), continuous wet (CW), and freeze/thaw (F/T)) in order to assess the self-healing capability of ECC mixtures incorporating different SCMs by measuring the chloride ion permeability of the ECC according to the ASTM C1202 (1997). Microstructural changes within the cracks were also analyzed using scanning electron microscopy (SEM) and video microscope. X-ray diffraction (XRD) analyses are also carried out in order to confirm the composition of chemical products necessary for self-healing.

1.2 Research Objectives and Scope

To monitor mechanical properties, chloride ion permeability and self-healing behavior of ECC mixtures, an experimental program based on mechanical pre-loading, different curing regimes and supplementary cementitious materials (SCMs) was planned. Three different mixtures were prepared with different mineral

admixtures. Specimens with water to cementitious material ratio (W/CM) of 0.27 and mineral admixture to Portland cement (MA/PC) ratio of 2.2 were produced. The ingredients used in ECC mixtures were CEM I 42.5 type ordinary Portland cement (PC), Class-F fly ash (F), Class-C fly ash (C), ground granulated blast furnace slag (S), sand, polyvinyl-alcohol fibers (PVA), water and high range water reducing admixture (HRWR).

Self-healing ability of the ECC specimens were observed through rapid chloride permeability test (RCPT), scanning electron microscopy (SEM) and video microscope with maximum enlargement of 125X. In addition, crack characteristics and microstructural changes in self healed cracks were analyzed with X-ray diffraction (XRD) technique. In terms of mechanical properties, the results of compression test, four point bending test and mid-span beam deflection values were discussed. Within the scope of the experimental test program, three curing conditions, continuous wet (CW), continuous air (CA), freeze/thaw cycle (F/T) and three pre-loading deformation levels, 0 mm, 1.00 mm, 1.25 mm, were applied to the specimens, respectively. As a result, this study contributes to the discussion of combined effect of different mineral admixtures, pre-loading deformation levels and curing conditions on the self-healing ability of ECC's. Together with the mechanical property enhancement, the substantial use of these waste materials from industrial processes is an important step toward sustainability in the construction industry.

In chapter 2, main mechanisms responsible for self-healing phenomenon, factors affecting it, methods to evaluate self-healing and pozzolanic materials such as fly ash and ground granulated blast furnace slag are discussed in detail. In chapter 3, experimental program, material properties and tests applied on the specimens are discussed. The results of the experimental studies are presented and discussed in Chapter 4. The conclusions of the research are presented in Chapter 5.

CHAPTER II

LITERATURE REVIEW AND BACKGROUND

2.1 Introduction

The self-healing phenomenon of cementitious composites has been observed in natural environments for many years. For concrete infrastructures, where water and CO₂ are available, concrete can heal its own damage with chemical products by itself. The main cause of self-healing is attributed to the formation of calcium carbonate, a result of reaction between calcium ion in concrete and CO₂ dissolved in water (Edvardsen, 1999; Cowie and Glassert, 1992). This type of self-healing mainly improves the transport properties, and is therefore the most important to impermeable structures, such as underground structures, water tanks, water channel and dams. Continuous hydration of unhydrated cementitious materials is another mechanism for the self-healing to occur (Ter Heide, 2005). Due to the limited volume of self-healing products, the crack width of the concrete material is found to be critical for self-healing to take place (Qian et al., 2009; Li and Yang, 2007). The requirement of crack width to promote self-healing falls roughly below 200 μm and preferably lower than 50 μm (Li and Yang, 2007) especially for self-healing based on ongoing hydration of unhydrated cementitious materials. Therefore tight crack width is one of the most important criteria to attain effective self-healing in cementitious materials.

Consistent control of the tight crack width, even with the presence of steel reinforcement is relatively difficult in reinforced concrete (R/C). Through the use of High Performance Fiber Reinforced Cementitious Composites (HPFRCC), which display significantly higher ductility than reinforced concrete (R/C), durability problems resulting from cracking may be solved (Wang and Li, 2007). Yet to prove acceptable for many applications, these materials must show high ductility without forming large cracks and enhanced material and structural durability by exhibiting such characteristics as excellent protection of steel reinforcement, resistance to freeze

thaw cycles, de-icing salt scaling resistance and demonstration of long term mechanical performance. The introduction of materials which provide both ductility and durability can significantly impact the design of future, more durable infrastructure systems.

2.2 Engineered Cementitious Composites (ECC)

As a new class of HPFRCC materials, Engineered Cementitious Composites (ECC) is a ductile fiber reinforced cementitious composite micromechanically designed to achieve high damage tolerance under severe loading and high durability under normal service conditions (Li, 1998; Li et al., 2001; Li, 2003). The most distinctive characteristic separating ECC from conventional concrete and fiber reinforced concrete (FRC) is an ultimate tensile strain capacity between 3% to 5%, depending on the specific ECC mixture. This strain capacity is realized through the formation of many closely spaced microcracks, allowing for a strain capacity over 300 times that of normal concrete. These cracks, which carry increasing load after formation, allow the material to exhibit strain hardening, similar to many ductile metals.

While the components of ECC may be similar to FRC, the distinctive ECC characteristic of strain hardening through microcracking is achieved through micromechanical tailoring of the components (i.e. cement, aggregate, and fibers) (Li, 1998; Lin et al., 1999; Li et al., 2001; Li, 2003), along with control of the interfacial properties between components. Fracture properties of the cementitious matrix are carefully controlled through mix proportions. Fiber properties, such as strength, modulus of elasticity, and aspect ratio have been customized for use in ECC. The interfacial properties between fiber and matrix have also been optimized in cooperation with the manufacturer for use in this material. Typical mix proportions of ECC using a poly-vinyl-alcohol (PVA) fiber are given in Table 2.1.

Table 2.1 Typical mix design of ECC material

Cement	Water	Aggregate	Fly Ash	HRWR*	Fiber (%)
1.00	0.58	0.80	1.20	0.013	2.00

*HRWR = High range water reducing admixture; all ingredients proportion by weight except for fiber.

While most HPFRCCs rely on a high fiber volume to achieve high performance, ECC uses low amounts, typically 2% by volume, of short, discontinuous fiber. This low fiber volume, along with the common components, allows flexibility in construction execution. To date, ECC materials have been engineered for self-consolidation casting (Kong et al., 2003a), extrusion (Stang and Li, 1999), shotcreting (Kim et al., 2003), and conventional mixing in a gravity mixer or conventional mixing truck (Lepech and Li, 2007).

Figure 2.1 shows a typical uniaxial tensile stress-strain curve of ECC material containing 2% poly-vinyl-alcohol (PVA) fiber (Weimann and Li, 2003). The characteristic strain-hardening behavior after first cracking is accompanied by multiple microcracking. The crack width development during inelastic straining is also shown in Figure 2.1. Even at ultimate load, the crack width remains smaller than 80 μm . This tight crack width is self-controlled and, whether the composite is used in combination with conventional reinforcement or not, it is a material characteristic independent of rebar reinforcement ratio. In contrast, normal concrete and fiber reinforced concrete rely on steel reinforcement for crack width control. Under severe bending loads, an ECC beam deforms similar to a ductile metal plate through plastic deformation (Figure 2.2). In compression, ECC materials exhibit compressive strengths similar to high strength concrete (e.g. greater than 60 MPa) (Lepech and Li, 2007).

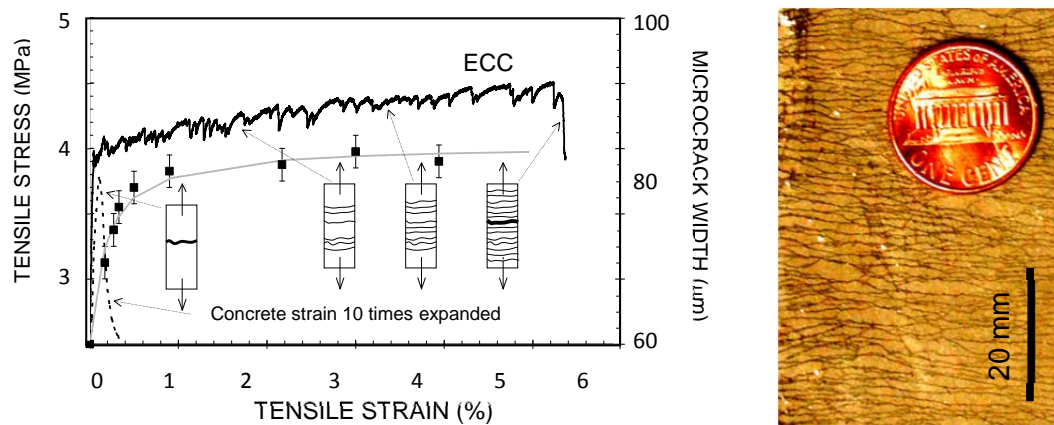


Figure 2.1 Typical tensile stress-strain curve and crack width development of ECC (Weimann and Li, 2003)

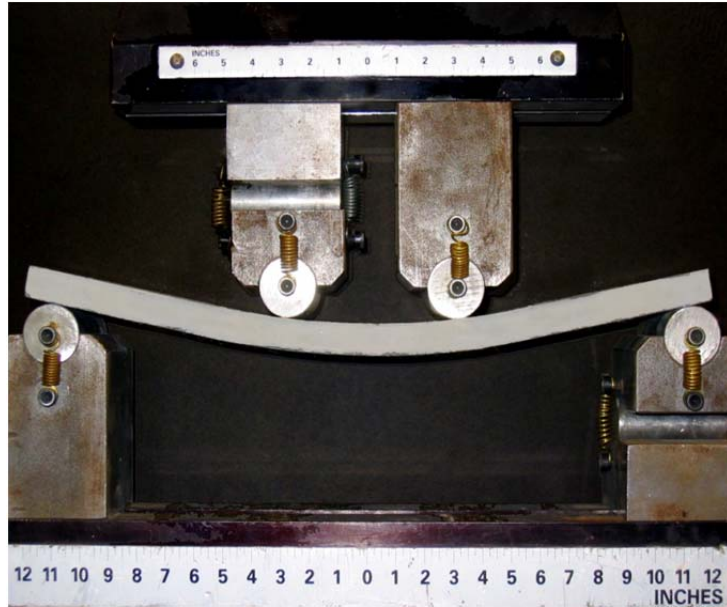


Figure 2.2 Response of ECC under flexural loading

2.3 Design of Engineered Cementitious Composites

In design of ECC material, primary purpose is to assure the occurrence of multiple cracking and strain hardening behavior under loading. Through the formation of multiple microcracks, large deformations are easy to be experienced over the span of specimen. Marshall and Cox (1988) first stated that, the formation of multiple microcracking and strain hardening behavior in ECC is dependent on steady state cracks to propagate. This finding then extended by Li and Leung (1992) and Lin et al. (1999) to be used in the case of fiber reinforced cementitious composites. Instead of Griffith-type cracks that open up while propagating as in typical tension-softening fiber reinforced cementitious materials, ECC material experiences large tensile strains in the strain hardening stage through the saturation of specimen with steady state “flat cracks” that keep crack width constant during the propagation. Fiber bridging stress versus crack width opening relation and the cracking toughness of mortar matrix are two main criterions that are responsible for the occurrence of multiple steady state cracking behavior. In order to obtain this behavior the inequality shown in Equation-2.1 must be fulfilled.

$$J'_b = \sigma_0 \delta_0 - \int_0^{\delta_0} \sigma(\delta) d\delta \geq J_{tip} \approx \frac{K_m^2}{E_m} \quad (2.1)$$

where J'_b is the complimentary energy shown in Figure 2.3, σ_0 and δ_0 are the maximum crack bridging stress and corresponding crack opening, J_{tip} is the fracture energy of the mortar matrix, K_m is the fracture toughness of the mortar matrix, and E_m is the elastic modulus of the mortar matrix. In addition to the fracture energy criterion, a strength criterion expressed in Equation-2.2 must be satisfied.

$$\sigma_0 > \sigma_{fc} \quad (2.2)$$

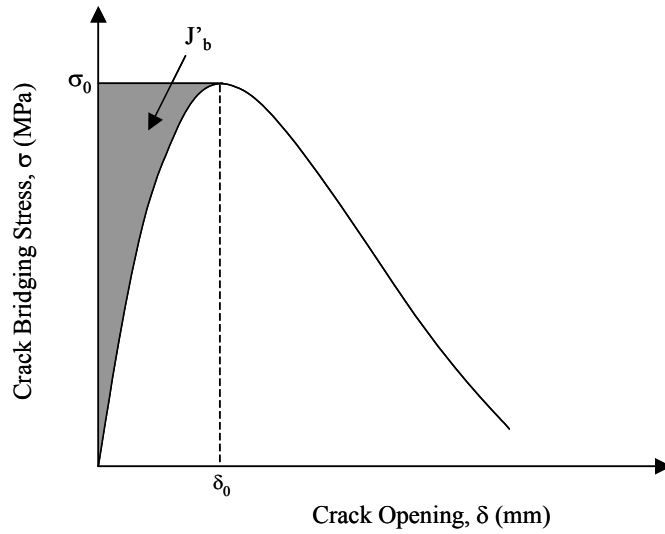


Figure 2.3 Crack bridging stress versus crack opening relation

where, σ_0 is the maximum crack bridging stress and σ_{fc} is the first cracking strength of the mortar matrix. For saturated multiple cracking, Wang and Li (2004) found that Equation-2.2 must be satisfied at each potential crack plane, where σ_{fc} is understood as the cracking stress on that crack plane.

Development of multiple steady state crack formation and strain hardening behavior can be well understood through the attainment of ECC mixture that adequately meets the two abovementioned parameters. However, along with the formation of steady state cracks, the material design must be made to obtain crack widths less than 100 μm threshold limit. This need can be satisfied with the tailoring of crack bridging versus crack opening relation stated in Equation-2.1. As shown in Figure 2.3, during the multiple microcracking of ECC material, the maximum steady state crack width can be regarded as δ_0 and the crack width accounting for the maximum crack bridging stress as σ_0 . Crack bridging stress starts to decrease, if crack width exceeds

δ_0 value. In this case, localized cracks start to occur and the formation of multiple steady state microcracks ceases. However, as δ_0 value is kept under 100 μm threshold, multiple microcracking and strain hardening behavior can be acquired.

Lin et al. (1999) proposed the formulation of the crack bridging stress versus opening relationship based on summing the bridging force contribution of fibers that cross a given crack plane. This relation is expressed in Equation-2.3.

$$\sigma(\delta) = \frac{4V_f}{\pi d_f^2} \int_{\phi=0}^{\pi/2} \left(\int_{z=0}^{(L_f/2)\cos\phi} P(\delta) e^{f\phi} p(\phi) p(z) dz \right) d\phi \quad (2.3)$$

where V_f is the fiber volume fraction, d_f is the fiber diameter, ϕ is the orientation angle of the fiber, L_f is the fiber length, z is the centroidal distance of a fiber from the crack plane, f is a snubbing coefficient, and $p(\phi)$ and $p(z)$ are probability density functions of the fiber orientation angle and centroidal distance from the crack plane, respectively. $P(\delta)$ is the pullout load versus displacement relation of a single fiber aligned normal to the crack plane, also described in Lin et al. (1999). The factor $e^{f\phi}$ accounts for the changes in bridging force for fibers crossing at an inclined angle to the crack plane.

Through the use of basic micromechanical models, ECC material can be tailored to endure larger strains up to several percent without the formation of larger cracks that could cause an increase in overall permeability. The application of material design procedures, such as those outlined above, allow materials engineers to carefully match material characteristics to specific structural demands, such as strain capacity and low permeability.

2.4 Self Healing in ECC

2.4.1 Conditions for Reliable Self-Healing

Previous researchers have engaged in highly regarded studies related to the phenomenon of concrete self-healing, the formation of self-healing products, and the necessary conditions to experience self-healing in concrete materials. Performed

studies indicated that, in order to obtain reliable self-healing behavior in concrete material, existence of certain chemical species, several environmental exposures and tight crack width are crucial. Even, there are some variations in the results individually, the general trend of these studies are obvious. In order for significant and reliable self-healing to take place, first, various environmental conditions are needed. These conditions may range from submersion in water to wet-dry cyclic exposures and they are existent for many infrastructure types. Another criterion for reliable self-healing to occur is the presence of adequate chemical species which are essential for self-healing mechanism. This requirement is also readily available due to the chemical composition of cementitious materials and unhydrated particles present in the cement paste along with the presence of CO₂ in both gas or dissolved-in-water form. In addition to the abovementioned criterions, however, crack width stands as the most important parameter for the occurrence of reliable self-healing. The crack width requirement is roughly 200 μm and ideally below 50 μm. This condition is significantly hard to achieve in a consistent manner and explains the reason behind ineffective self-healing behavior in most cementitious composites. Therefore, with its inherent tight crack width ECC stands as a quite promising material solution.

2.4.2 Effect of Crack Width on Self-Healing

The influence of crack width on the self-healing capability was observed by Yang et al. (2009). To do this mortar specimens measuring 230x76x13 mm with 0.5% (in volume) poly vinyl alcohol (PVA) fiber were prepared to obtain tension softening behavior. These specimens were prepared to take advantage of tension softening behavior with single crack. Uniaxial tension tests were then conducted on the specimens to obtain single crack having crack width between 0 to 300 μm. After introducing the microcracks, specimens were subjected to 10 wet-dry cycles (CR1, (submersion in water at 20 °C for 24 h and drying in laboratory air at 21°C ± 1 °C, 50% ± 5% RH for 24 h). As seen in Figure 2.4, crack width stands as a significant parameter in realizing the self-healing behavior in terms of the resonant frequency (RF) measurements. It is clear from the authors' findings that after the wetting and drying cycles, cracks having the widths less than 50 μm was fully recovered the RF

values. On the other hand, no improvement in RF values was observed for the cracks having crack widths more than 150 μm .

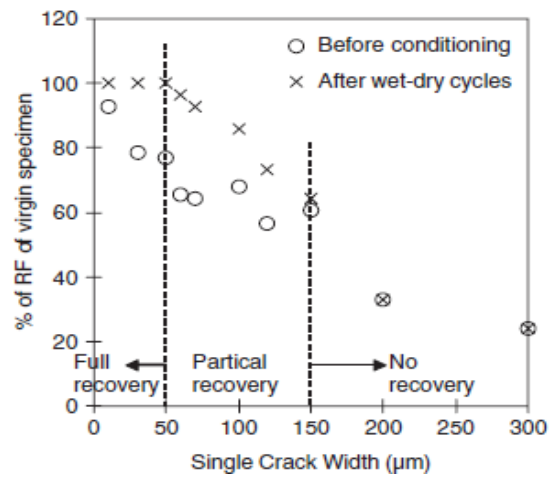


Figure 2.4 Resonant frequency (RF) ratio as a function of crack width (Yang et al., 2009)

Along with the RF measurements, permeability measurements were made on the same specimens and results were recorded in terms of permeability coefficients. As seen in Figure 2.5, after 10 wetting and drying cycles, cracks having the widths of less than 50 μm behaved almost like virgin specimens in terms of permeability.

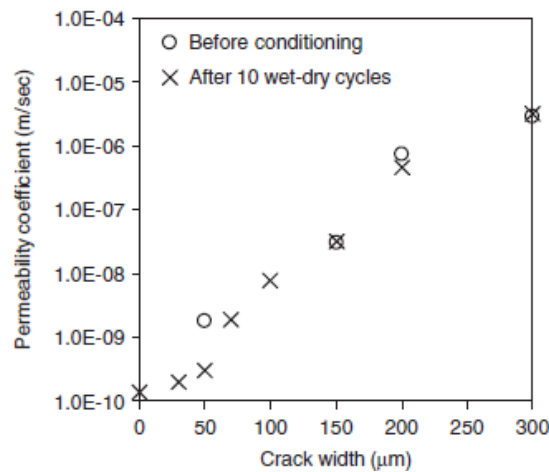


Figure 2.5 Permeability coefficient as a function of crack width before and after conditioning (Yang et al., 2009)

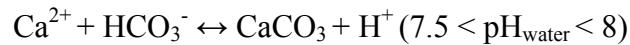
As a result, it was concluded that in order to have a complete self-healing in cementitious composites in both mechanical and transport properties, the crack widths must be restricted below 50 μm .

2.4.3 Self-Healing Mechanism

In the literature (Clear, 1985; Meichsner, 1992; Guppy 1998) the following chemical, physical and mechanical processes were listed as the probable reasons of autogenous self-healing:

- Swelling and hydration of cement paste;
- Precipitation of calcium carbonate (CaCO_3) crystals;
- Blocking of flow path by impurities in water; and
- Blocking of flow path by the broken concrete particles.

Among all, the precipitation of CaCO_3 was found to be the most important reason that affects self-healing behavior in concrete (Edvardsen, 1999). Calcite formation in the area of water bearing cracks takes place in the material system $\text{CaCO}_3\text{-CO}_2\text{-H}_2\text{O}$ according to the following reactions (Cowie, 1992; Garrels and Christ, 1965).



The water-insoluble CaCO_3 is evolved from a reaction between the calcium ions Ca^{2+} coming from the concrete itself and the in-water available bicarbonates HCO_3^- or carbonates CO_3^{2-} . Apart from the temperature, pH value and CO_2 partial pressure, calcite crystal growth depends very decisively on the saturation index (Ω) of calcite [$\Omega = (\text{Ca}^{2+})(\text{CO}_3^{2-})/\text{K}_c$] where (Ca^{2+}) and (CO_3^{2-}) are the ion concentrations in the solution and K_c is the solubility product of calcite (Nancollas and Reddy, 1971). Furthermore, thermodynamic considerations of CaCO_3 formation imply that rising temperature and pH value and decreasing partial CO_2 pressure of water favor CaCO_3 precipitation in a crack.

2.4.4 Self-Healing Examination Methods

2.4.4.1 Dynamic Modulus Measurements

In order to evaluate the rate of self-healing dynamic modulus measurement depending on ASTM C215 seems to be a good gauge. This test is based on the changes in resonant frequency (RF) and it was proven as a promising technique for the determination of deterioration due to frost action as referenced in ASTM C666. Instead of quantifying the damage, it is utilized to observe the materials' self-healing ability as a diminishment in material damage especially in the case of cracked specimens (Yang et al., 2005).

To create an understanding on the dynamic modulus measurements related to self-healing determination, ECC coupon specimens with the dimensions of 230x76x13 mm were prepared and pre-deformed to several uniaxial deformation levels (ranging between the values of 0.3% and 3%) at the age 6 months (Li and Yang, 2007). Depending on the pre-deformation level small crack closures (15-20%) were observed on the specimens upon unloading. After, same specimens were subjected to wet-dry cycles. In Figure 2.6-a and b, resonant frequency values of ECC specimens pre-deformed to different strain levels under wet-dry cycles of CR1 (submersion in water at 20 °C for 24 h and drying in laboratory air at 21°C ± 1 °C, 50% ± 5% RH for 24 h) and CR2 (submersion in water at 20°C for 24 h, oven drying at 55 °C for 22 h, and cooling in laboratory air at 21°C ± 1°C, 50% ± 5% RH for 2h), were shown, respectively.

The shaded area shows the resonant frequency interval of ECC specimens exposed to the same wet-dry cycles. It was observed from the figures that regardless of curing type, all ECC specimens showed a gradual recovery in resonant frequency values. It was clear from the findings of authors that after 4 to 5 cycles, resonant frequencies stabilized. This means that 4-5 wet-dry cycles were sufficient for engaging marked self-healing in pre-deformed ECC specimens. As expected, specimens with higher uniaxial pre-deformation levels exhibited lower initial and final resonant frequency values due to higher damages experienced in terms of multiple crack formation.

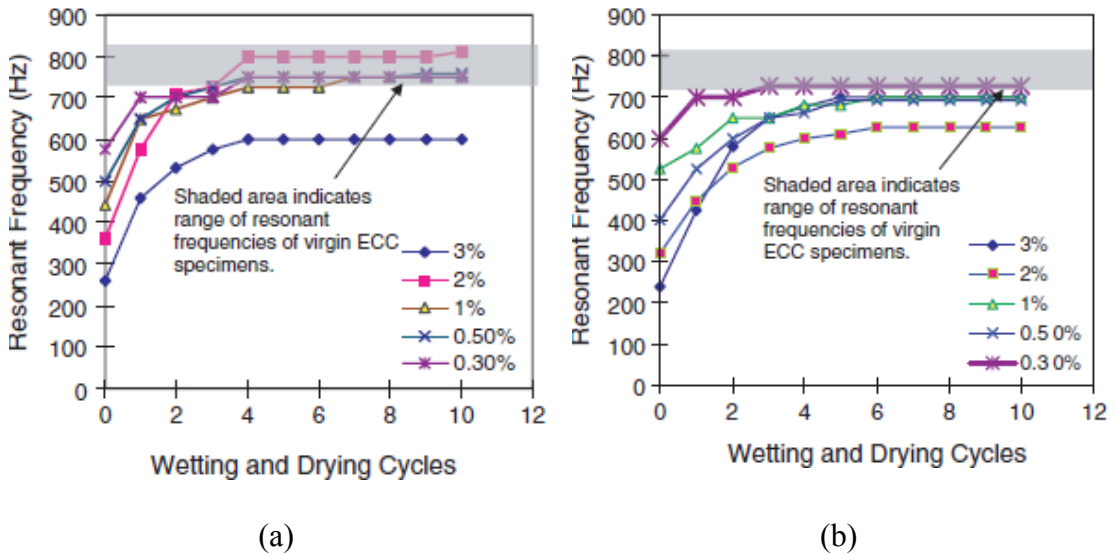


Figure 2.6 Self-healing rate of ECC under cyclic wetting and drying: (a) Resonant frequency recovery under CR1 (water/air cycle); (b) Resonant frequency recovery under CR2 (water/hot air cycle) (Li and Yang, 2007)

As it is seen from Figure 2.7, without the addition of increases in resonant frequency values due to further hydration, ultimate resonant frequency values either approached or exceeded 100% of initial resonant frequency and for some specimens even reached to 110% level.

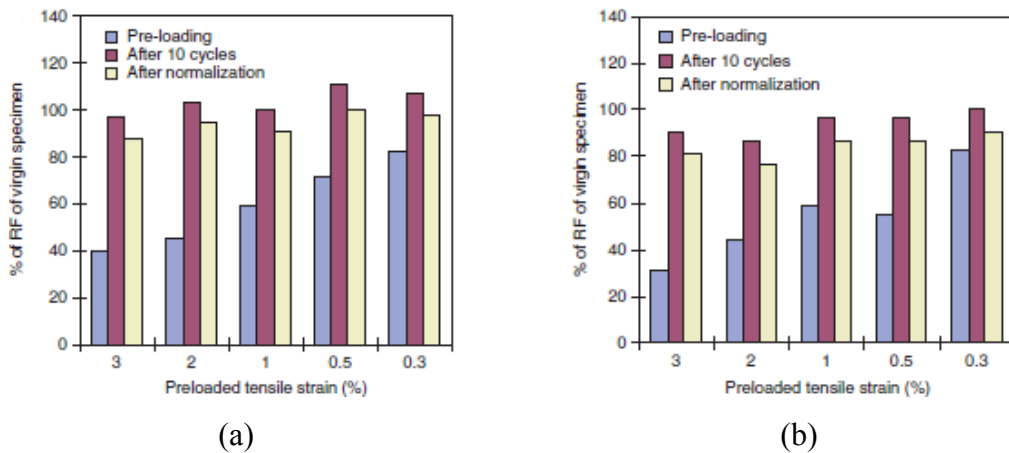


Figure 2.7 Extent of self-healing in ECC under cyclic wetting and drying: (a) Extent of self-healing in ECC under CR1 (water/air cycle); (b) Extent of self-healing in ECC under CR2 (water/hot air cycle) (Li and Yang, 2007)

In order to normalize the results and not to have contradictory results, increases caused by hydration processes were excluded. To do this, resonant frequencies of

pristine ECC specimens were evaluated for 10 wet-dry cycles under the abovementioned conditions (CR1 and CR2) and final results were calculated. After the normalization of results, under CR1 conditioning, while 40-82% of recovery in the resonant frequency values was observed after pre-cracking, these values increased to 81-100% of initial value after exposing to the wet-dry cycles for the same specimens. However, for CR2 curing condition, recovery in initial values was 31-83% and 77-90% of initial resonant frequency values before and after exposure to the wet-dry cycles.

As it is more evident from Figure 2.7 that marked difference exists between the resonant frequency values of specimens exposed to CR1 and CR2 curing conditions indicating the attainment of specimens' self-healing behavior. The reason behind higher initial dynamic modulus recovery levels in the case of CR1 conditioning might be correlated with the effects of temperature. Since specimens were dried in oven at 55 °C in the case of CR2 curing condition, it is reasonable to say that while water in the pores was evaporating, it built internal vapor pressure causing microcracks in the matrix which are coupled with the effect of further mechanical pre-deformation. With the combined effects of both mechanical and internal microcracking, lower recovery or self-healing levels in the case of CR2 curing condition are more comprehensible.

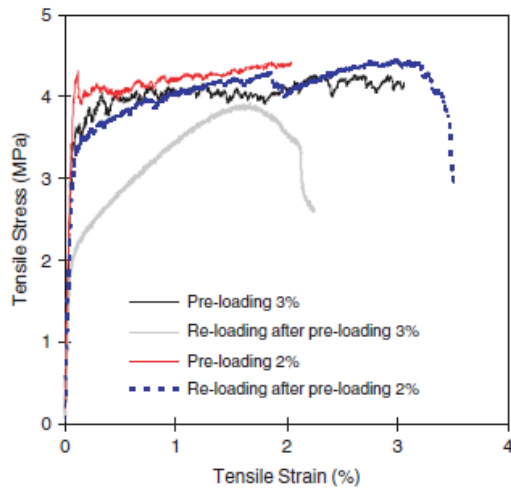
2.4.4.2 Uniaxial Tensile Test

Tensile strain hardening behavior stands as one of the intrinsic characteristic of ECC material that separates it from the conventional concrete. Li and Yang (2007) conducted a research to evaluate the quality of self-healing behavior in strain hardening materials by checking the change in mechanical properties. In order to do this, ECC specimens having the dimensions of 230 x 76 x 13 mm were prepared and pre-deformed to different deformation levels ranging between 0.3% and 3% with the help of uniaxial tension test at the age of 6 months. The loading rate of the tension test was 0.0025 mm/s (Figure 2.8).

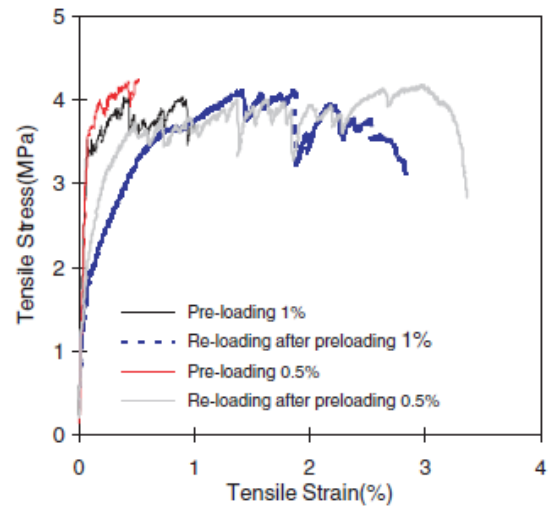


Figure 2.8 Uniaxial tensile test set up

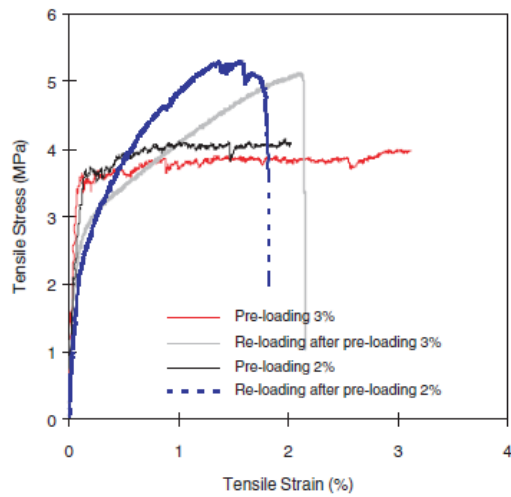
To facilitate the gripping of specimen holding devices, aluminum plates were glued both sides at the ends of coupon specimens. The deformation of specimens was measured with the help of two attached external linear variable displacement transducers. After exposure to CR1 and CR2 wet-dry cyclic conditioning, specimens were reloaded under uniaxial tension test for analyzing the improvement in the stiffness, tensile strength and deformation capacity. The results drawn from this study indicated that after curing process, specimens exposed to CR1 curing condition showed a tensile strain capacity ranging between 1.7% and 3.1%. For the specimens exposed to CR2 curing condition, however, the results decreased to 0.8 and 2.2% (Figure 2.9). On the other hand, ultimate tensile strength values were found to be lower for CR1 curing condition compared with CR2. This trend was found attributable to the probable effect of CR2 curing that is composed of submersion in water and then drying in oven 50 °C.



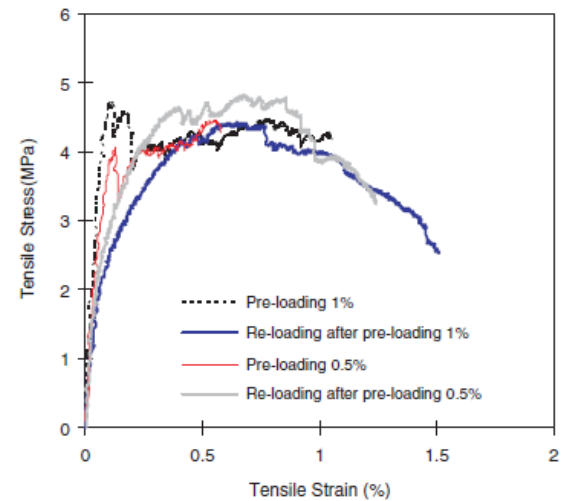
(a)



(b)



(c)



(d)

Figure 2.9 Preloading and reloading after 10 CR1 (water/air) cycles tensile stress–strain relations of ECC specimens: (a) Specimen with preloading above 1%; (b) Specimen with preloading to or below 1%, Preloading and reloading after 10 CR2 (water/hot air) cycles tensile stress–strain relations of ECC specimens: (c) Specimen with preloading above 1%; (d) Specimen with preloading to or below (Li and Yang, 2007)

It was claimed by the authors that with the help of temperature, the water inside the pores will be evaporated and provide steam curing which would lead to further hydration of unhydrated cementitious particles and increased total ultimate tensile strength through the refinement of bond strength. In addition, with the increase in interfacial bonding, fibers present in the system tend to rupture instead of a pull out

leading to lower tensile ductility and adverse effects on the development of multiple cracking in the case of CR2 curing condition.

In the cited study, it has been also shown that ECC specimens that were preloaded to the 2% and 3% deformation levels showed significant difference in stiffness values compared with the specimens reloaded after preloading. As seen in Figure 2.10-a, elastic modulus values were significantly decreased on reloading and the effect was even more severe when the preloading level was increased. The reason for this behavior was found attributable to the reopening of the cracks. The effects of different environmental conditions on the recovery of elastic modulus values were also discussed in the same study. As it is seen from Figure 2.10-b, significant amount of recovery was attained in the stiffness values regardless of curing condition implying that self-healing occurred in ECC material may result not only the sealing of cracks but true rehabilitation of mechanical properties.

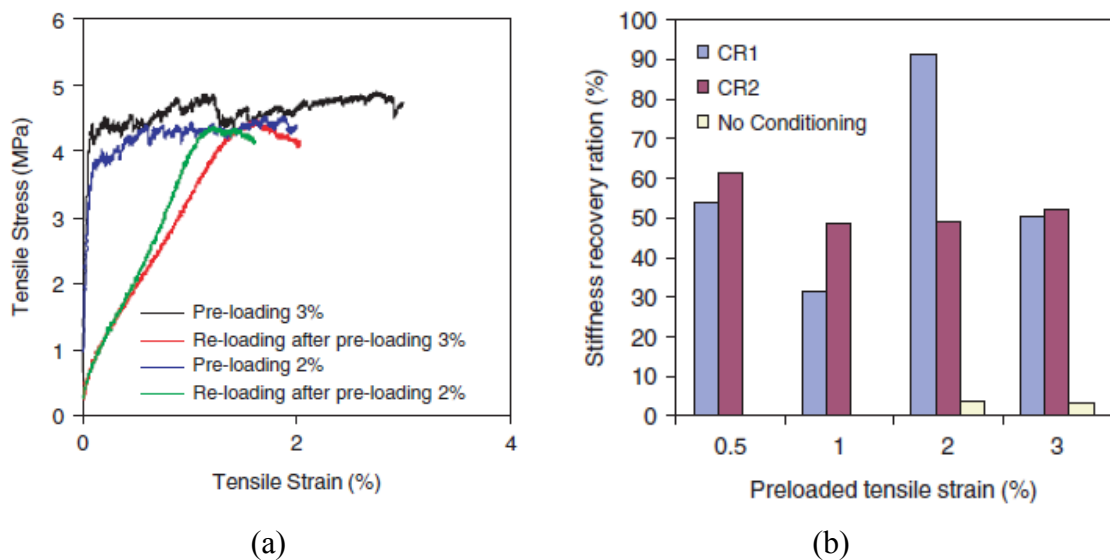


Figure 2.10 (a) Preloading and reloading without self healing tensile stress–strain curve of ECC specimens, (b) Stiffness recovery of ECC under different conditioning regime (Li and Yang, 2007)

2.4.4.3 Water Permeability Test (WPT)

Transport mechanisms of fluids within concrete have been of interest due to their substantial effects on durability. In hardened concrete, significant works have been undertaken with respect to the transport mechanisms of permeability, absorption, and

diffusion. Though, numerous studies have been conducted on the concrete members in uncracked state (Perraton et al., 1988; Powers, 1991; Reinhardt et al., 1997) ,in real field conditions it is inevitable not to have cracks in concrete material itself that might drastically change the transportation properties. Therefore, it is vital to create an understanding on transport mechanisms for both cracked and uncracked concrete materials in favor of obtaining durable infrastructures.

To account for the permeability properties of ECC, an experimental study was undertaken by Lepech and Li (2009). In the scope of the study, water permeability of mechanically loaded ECC and reinforced mortar specimens was studied. While a falling head test setup was used for specimens having low permeability, for specimens with high permeability (i.e. large crack width) a constant head test setup was chosen. In Figure 2.11 test setups for proposed permeability tests were displayed.

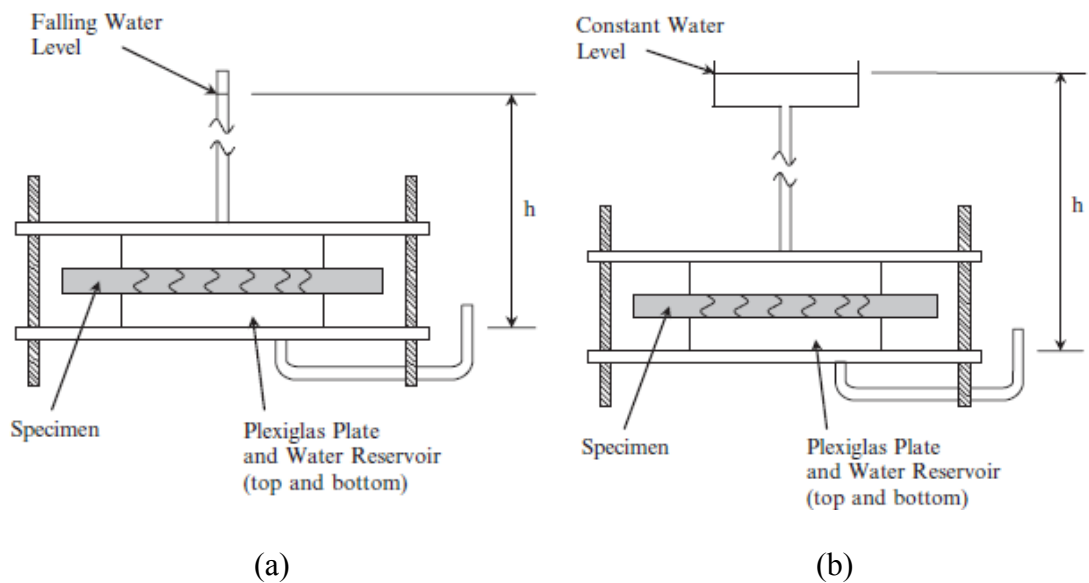


Figure 2.11 (a) Falling Head Permeability Test Setup (Cernica, 1982) (b) Constant Head Permeability Test Setup (Wang et al., 1997)

The equations that were used while calculating the permeability for specimens in the falling head and constant head tests were shown in Equation 2.4 and 2.5, respectively.

$$k = \frac{a \cdot L}{A \cdot t_f} \left(\frac{h_0}{h_f} \right) \quad (2.4)$$

$$k = \frac{V \cdot L}{A \cdot h_0 \cdot t_f} \quad (2.5)$$

where k is the coefficient of permeability, a is the cross sectional area of the standpipe, L is the specimen thickness in the direction of flow, A is the cross sectional area subject to flow, t_f is the test duration, h_0 is the initial hydraulic head, h_f is the final hydraulic head, and V is the volume of liquid passed through the specimen during the test.

In this study, to assure the complete saturation, specimens submerged in water for 14 days before permeability tests. As seen in Figure 2.12, regardless of strain level, permeability coefficient was stabilized in time. This behavior was found attributable to the significantly low water to binder ratio and large cementitious material content in the ECC mixture. It is well known that substantial amount of unhydrated cementitious materials present in the system stand as a big potential for self-healing phenomenon to take place, especially in the presence of water. This mechanism is more pronounced for ECC due its inherent tight crack width that promotes the occurrence of self-healing. As seen in Figure 2.13, white residue near the crack flanks was observed in ECC specimens after permeability tests implying the formation of new self-healing products. Refinement in permeability coefficient is more understandable by looking Figure 2.13 due to certain amounts of crack closure in time.

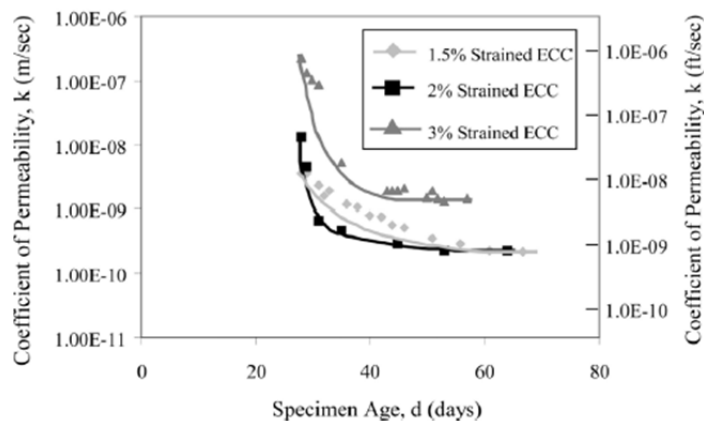


Figure 2.12 Development of Permeability for ECC Strained to 1.5%, 2%, and 3% (Lepech and Li, 2009)

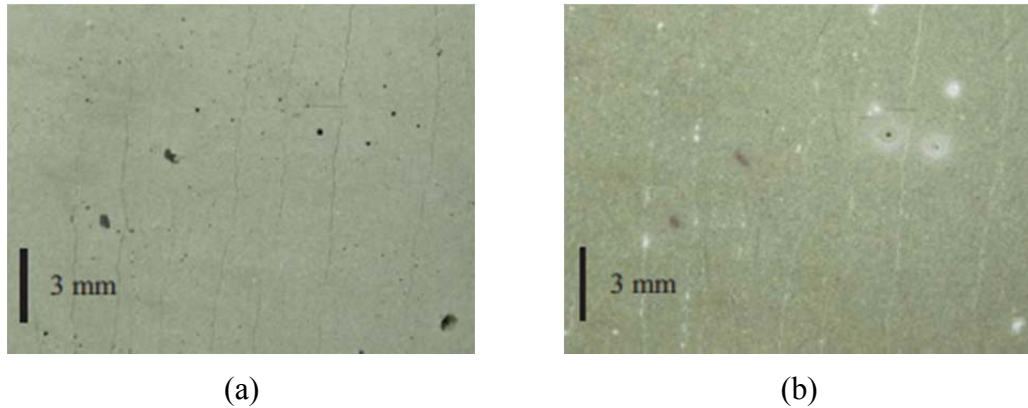


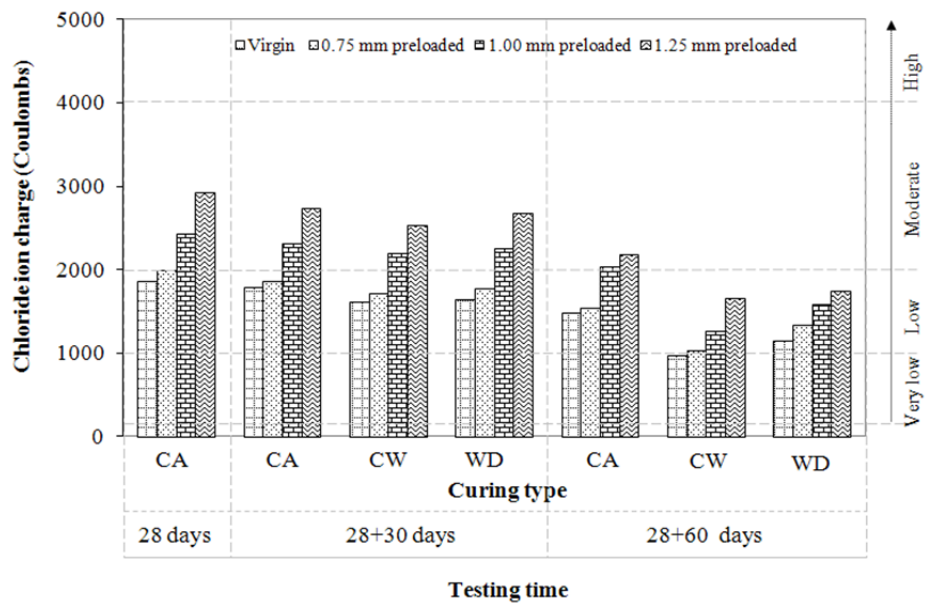
Figure 2.13 Appearance of ECC permeability specimens: (a) before permeability testing and (b) after permeability testing (Lepech and Li, 2009)

2.4.4.4 Rapid Chloride Permeability Test (RCPT)

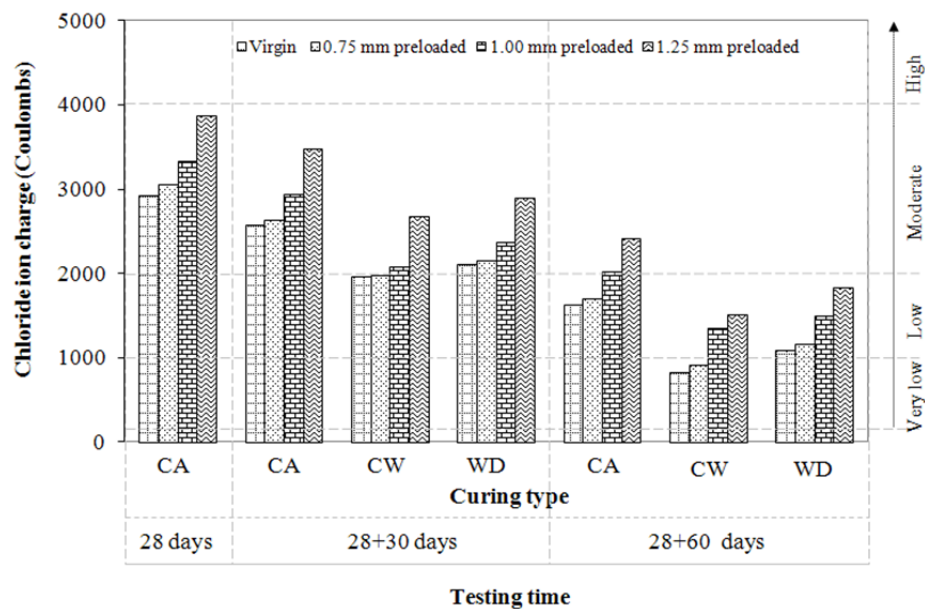
Misra et al. (1994) have stressed that chloride permeability as measured from RCPT can be used for quality control of concrete. It can be stated that, the total charge passed, in coulombs, is related to the ability of ECC specimens to resist chloride ion penetration. In other words, as more chloride ions migrate into the ECC specimen, more current can pass through. A high value for total charge passed indicates that the ECC is highly penetrable.

Self-healing behavior of high volume fly ash (HVFA – incorporating FA amount of %50, ECC-1 and %70, ECC 2) ECC specimens preloaded to different deformation levels (ranging from 0.75 mm to 1.00 mm) under different environmental conditions was observed in terms of RCPT results by Ozbay et al. (2012) The results taken from the experimental study indicated that different from the water penetration properties of microcracked ECC specimen (Lepech and Li, 2009) preloading affected the chloride ion penetration of the ECC specimens irrespective of the preloading level. When the FA content used in the production of ECC is increased, the increase in chloride ion permeation properties is less influenced from the mechanical preloading which may be correlated with the fact that an increase in the FA content in ECC production caused a reduction in the residual crack width from about 70 μm level to 40 μm level. There was also clear refinement in the RCPT results with further curing of specimens. As seen in Figure 2.14, chloride ion permeability results were decreased significantly with time implying the occurrence of great deal of self-

healing. This trend was even more obvious for ECC-2 specimens. The probable reason for this behavior is attributable to the higher amounts of unhydrated fly ash particles present in ECC-2. In addition, the improvement in RCPT results was found much more evident after exposure to continuous wet curing condition showing that water is the key parameter for substantial amount of self-healing to take place.



ECC-1



ECC-2

Figure 2.14 Chloride ion permeability values of the ECC mixtures under different curing conditions and testing ages Ozbay et al. (2012)

2.4.4.5 Microscopic Observation and Analysis

It is probable that quality of self-healing is affected by the products formed inside the crack. Analyses of these products were conducted using scanning electron microscopy (SEM) and energy dispersive X-ray analysis (EDX) techniques. The crystalline and chemical properties of self-healing products were determined. The techniques listed above are especially useful to verify the chemical makeup of self-healing compounds that are necessary for identifying the chemical precursors to self-healing and ensuring their presence within the composite.

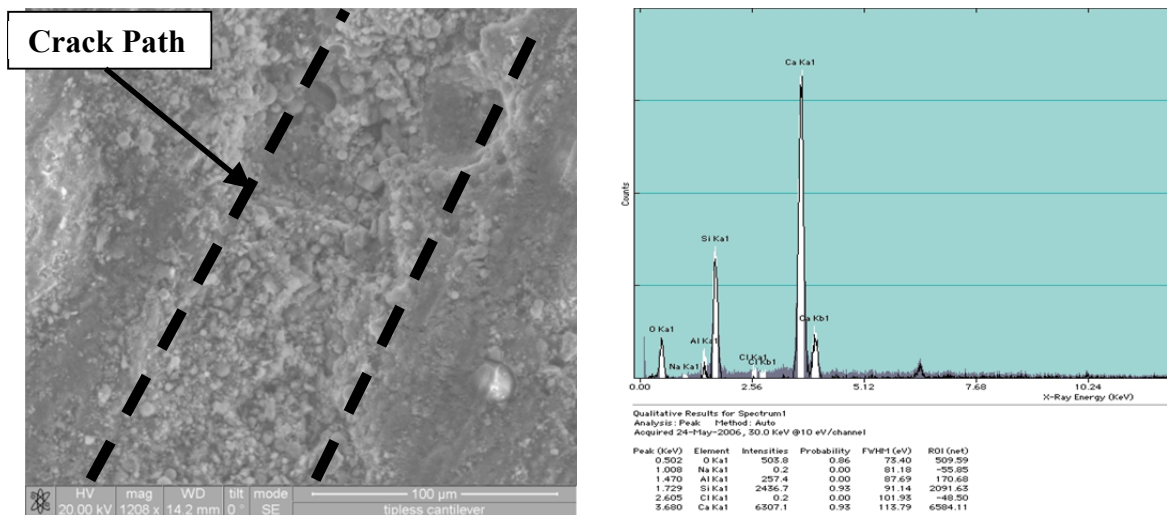


Figure 2.15 SEM micrograph with EDX pattern of rehydration products in a self-healed crack (ECC-2, after 60 days moist curing) Ozbay et al. (2012)

Ozbay et al. (2012) concluded that most of the products seen in the self-healed cracks after curing were the deposition of calcium carbonate and newly formed C-S-H gels. The rehydration products within the healed cracks were shown in Figure 2.15. Certain chemical species such as carbonates or bicarbonates must be present in the crack flanks to facilitate the calcium carbonate precipitation. The results drawn from this study indicated that during the curing process, with the help of water and CO₂ dissolved in it, formation of calcium carbonate was triggered for water cured specimens. However, the situation was not the same for air cured specimens. It is clear from the findings of the authors that with the absence of constant carbonate supply as in air cured specimens, limited amount of self-healing is attainable. On the

other hand, in the same study, distinct white residue that is probably caused due to the formation of efflorescence through leaching of calcium hydroxide (CH) was observed over the cracks. These observations indicated that microcracks of ECC-2 (FA/C=2.2) specimens were healed considerably after exposing to continuous water curing up to 60 days. The probable reason behind this behavior was found attributable to the large fly ash content and significantly low water to cementitious material ratio present in ECC mixture. The continued pozzolanic activity of fly ash and calcium carbonate formation are responsible for the self-healing.

2.5 Pozzolanic Material

According to ACI 116R-90 (1994), pozzolan is “a siliceous or siliceous and aluminous material, which in itself possesses little or no cementitious value but will, in finely divided form and in the presence of moisture, chemically react with calcium hydroxide at ordinary temperatures to form compounds possessing cementitious properties.” Mineral admixtures that are, or both cementitious and pozzolanic can be replaced with Portland cement. Some of the most used materials are ground granulated blast furnace slag (slag hereafter), fly ash, condensed silica fume. When properly used as a portion of the cementitious material, these pozzolanic admixtures can improve the properties of the fresh and hardened concrete.

Although several types of supplementary cementitious materials exist, the focus of this review will be on the two types used in this study, namely slag and fly ash. A brief overview of the history, properties, and usage of granulated blast furnace slag and fly ash in concrete is presented in Sections 2.6.1 and 2.6.2.

2.5.1 Slag

Slag has been used as partial replacement for Portland cement in concrete for more than 100 years (Glasser, 1991). As a by-product of the pig iron industry, slag is produced in large quantities in many areas around the world. In the United States, slag is most commonly used as base course for roads and other structures. However, in many other countries, most of the available slag is ground to approximately the

same fineness as cement and then utilized as a partial replacement for Portland cement in concrete.

The composition of slag can vary considerably between production facilities. The presence of the major oxides are typically found to be within the following ranges: magnesium oxide (MgO), 0 to 21 %; aluminum oxide (Al_2O_3), 5 to 33 %; silicon dioxide (SiO_2), 27 to 42 %; and calcium oxide (CaO), 30 to 50 % (Taylor, 1997). Although the composition of slag is important, the method used in its production is perhaps more important as air-cooled slag has very limited, if any, cementing properties (Moranville-Regourd, 1998). However, if the slag is cooled rapidly from its liquid state at 1350-1550 °C down to about 800 °C, crystallization of the material can be avoided and the resulting product often contains over 95% glass which is a latent hydraulic cement (Taylor, 1997).

For any substantial reaction to occur between slag and water, an activator is required. High alkaline environments have proved to be suitable activators. Fortunately, the pore solution of cement paste is basically composed of alkaline hydroxides and as such, provides for an excellent activator. The use of slag in concrete tends to slow down the rate of hydration at early ages at room temperature. However, elevated temperatures help activate the slag and increase the rate of hydration (Roy, 1992). Therefore, slag can be used in steam-cured concrete. In addition, the damaging effects, such as reduced strength and increased permeability, of high early age temperature on concretes containing slag are less pronounced than when slag is not used (Neville, 1996).

The reaction of a blend of cement and slag results in a higher percentage of calcium-silicate-hydrate (C-S-H) and less calcium hydroxide than plain cement (Neville, 1996). This alteration in the hydration products is attributable to the higher silicon content of the cement and slag blend when compared with plain cement. The change in the microstructure and the slower rate of hydration when slag is used typically yields denser and less permeable concretes.

In addition to lower permeability, concretes made with slag tend to have better resistance to chloride ion penetration than normal concretes. The freeze-thaw resistance of concrete made with slag is believed to be adequate and not adversely

affected when compared with concrete made without slag (Neville, 1996). However, concretes made with slag generally suffer higher degree of deicing salt scaling than do reference concretes made without slag (Stark and Ludwig, 1997b). Consequently, ACI Committee 318 (2002) limits the maximum amount of slag to 50 % of the total binder content if the concrete will be exposed to deicing chemicals. The total amount of slag and other supplementary cementitious materials is also limited to a maximum of 50 % of the total binder content.

2.5.2 Fly Ash

Fly ash is the most widely used mineral admixture for concrete. It is a byproduct of burning pulverized coal, in electric power production. During combustion, most of the volatile matter and carbon is burned off leaving the coal's mineral impurities (clay, feldspar, quartz, and shale) behind which then fuse together while in suspension. The fused particles are carried away by the exhaust by electrostatic precipitators or bag filters. During this process the fused material cools and solidifies to form the spherical fly ash particles. Typical particle size is around 20 microns but may range from one micron up to as large as 100 microns. Surface area may range from 200-700 m²/kg but typically are between 300-500 m²/kg (Kosmatka and Panarese, 1988).

Fly ash consists primarily of silica, aluminum, iron, and calcium in a silicate glass form. Minor constituents can be found in the form of magnesium, sulfur, sodium, potassium, and carbon. According to American Society for Testing and Materials (ASTM), there are two classes of fly ash (Table 2.2): Class C, which is normally produced from lignite or subbituminous coals and Class F, which is normally produced from bituminous coals (ASTM C 618, 2003). Class C fly ashes differ from Class F fly ashes in that they are self-hardening even without the presence of cement.

Table 2.2 Specifications for fly ash (ASTM C 618, 2003)

Class of Ash	ASTM Specification
Class C	SiO ₂ + Al ₂ O ₃ + Fe ₂ O ₃ > 50%
Class F	SiO ₂ + Al ₂ O ₃ + Fe ₂ O ₃ > 70%

CHAPTER III
EXPERIMENTAL PROGRAM

3.1 Materials

3.1.1 Portland Cement

The cement used in all mixtures was a normal portland cement CEM I 42.5R (PC), which correspond to ASTM Type I cement. It had a specific gravity of 3.06 and Blaine fineness of 325 m²/kg. Chemical composition and physical properties of cement are presented in Table 3.1.

Table 3.1 Chemical properties of Portland cement, fly ashes and slag

Chemical Composition	PC	F	C	S
CaO	61.43	3.48	15.50	35.09
SiO ₂	20.77	60.78	46.97	37.55
Al ₂ O ₃	5.55	21.68	11.86	10.55
Fe ₂ O ₃	3.35	5.48	7.98	0.28
MgO	2.49	1.71	6.51	7.92
SO ₃	2.49	0.34	3.47	2.95
K ₂ O	0.77	1.95	3.23	1.07
Na ₂ O	0.19	0.74	2.33	0.24
Loss on Ignition	2.20	1.57	0.45	2.79
SiO ₂ +Al ₂ O ₃ +Fe ₂ O ₃	29.37	87.94	66.81	48.38
Physical Properties				
Specific Gravity	3.06	2.10	2.27	2.79
Blaine Fineness (m ² /kg)	325	269	306	425

The particle size distributions of cement, obtained by a laser scattering technique, is given in Figure 3.1.

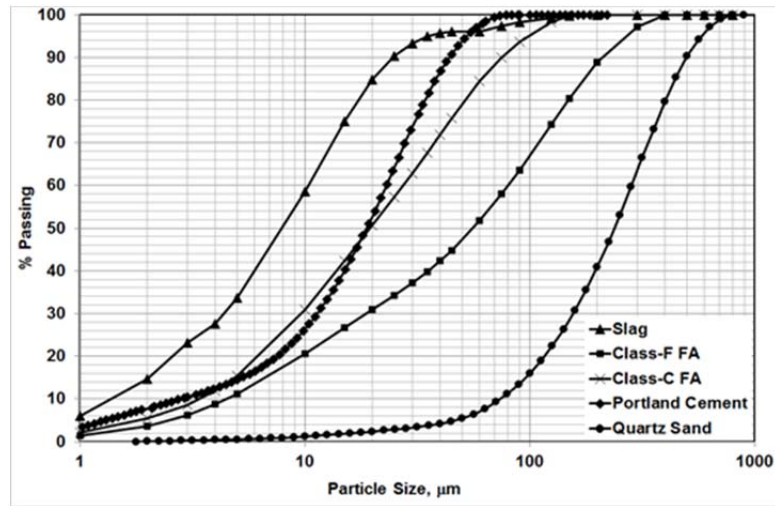


Figure 3.1 Particle size distributions of sand, portland cement and SCMs

3.1.2 Mineral Admixtures

3.1.2.1 Class-F Fly Ash

Class-F fly ash (F) conforming to (ASTM C 618, 2003) requirements with a lime content of 3.48% obtained from Sugözü Thermal Power Plant was used. The chemical properties of FA are given in Table 3.1. The specific gravity and Blaine fineness of FA are 2.10 and 269 m²/kg, respectively. The particle size distribution of FA is provided in Figure 3.1. Figure 3.2 illustrates the particle morphology of the FA. The scanning electron microscope (SEM) image showed that the particles of FA had significantly smooth spherical particles in comparison to slag.

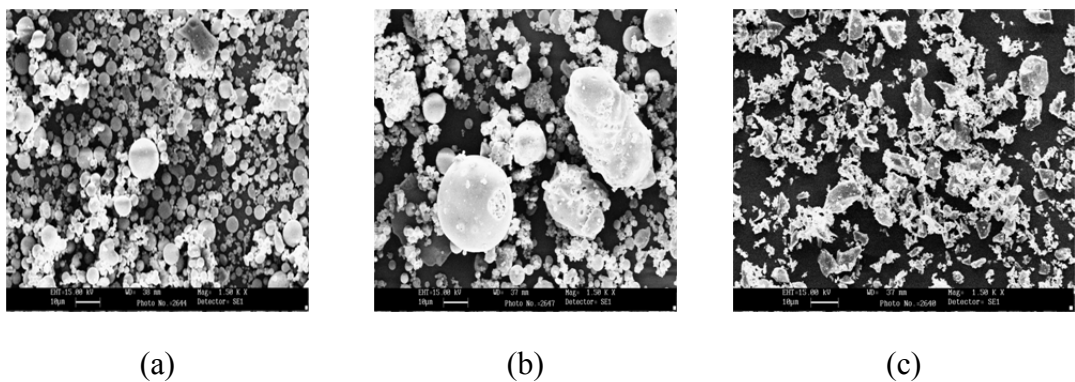


Figure 3.2 Particle morphology of a) Class-F fly ash b) Class-C fly ash c) slag determined by SEM

3.1.2.2 Class-C Fly Ash

Class-C fly ash (C) having specific gravity of 2.27 g/cm^3 and Blaine fineness of $306 \text{ m}^2/\text{kg}$ was obtained from Soma Thermal Power Plant in Turkey. It fulfills the requirements obligated by ASTM C618 (2003) with the total SiO_2 , Al_2O_3 and Fe_2O_3 proportion of more than %50. The particle size distribution and particle morphology of the FA were displayed in Figure 3.1 and 3.2, respectively.

3.1.2.3 Slag

Slag (S) was supplied from Iskenderun Iron–Steel Factory in Turkey. Its chemical oxide composition is given in Table 3.1. The specific gravity of slag was 2.79 g/cm^3 . The slag was ground granulated in Iskenderun Cement Factory to have a Blaine specific surface area about $425 \text{ m}^2/\text{kg}$. According to ASTM C989 (2009) hydraulic activity index, the slag used was classified as a category 80 slag. Particle size distribution of slag obtained by using the laser diffraction is shown in the Figure 3.1. To identify morphological characteristics of slag, it was analyzed with SEM and the resulting photograph is presented in Figure 3.2.

3.1.3 Aggregate

According to micromechanic-based design of ECC, exhibiting ductile and showing a large crack number, but small in width, of cementitious composites a low toughness of the matrix is required. However, with the increasing of maximum grain size of aggregate, increase in toughness of the matrix is appeared and as a result, to obtain suitable ECC, aggregate grain size is limited (Li et al., 1995). Therefore, so far, ECC has been produced successfully with an average grain size of about $110 \mu\text{m}$ (Li et al., 1995). Using high volumes of industrial by-product in the production of ECC decreases matrix toughness and provides freedom of changing aggregate size. It is very important to produce ECC from normal size local sources of aggregate in terms of widespread application for both literature and our country. For this purpose, in the production of ECC, fine quartz with the maximum aggregate size (MAS) of $400 \mu\text{m}$ was obtained from local sources in our country's resources. Water absorption

capacity and specific weight of quartz aggregate used is 0.3% and 2.60, respectively. The grain size distribution curves for these aggregates are presented in Figure 3.1.

3.1.4 Chemical Admixtures

To improve the workability of ECC mixtures, Glenium 51, high range water reducing admixture (HRWR – polycarboxylate ether as an active ingredient with 1.1 specific gravity and 40% solid content) produced by BASF Construction Chemicals was used.

3.1.5 Polyvinyl Alcohol (PVA) Fiber

Although different types of fibers have been utilized for the production ECC, PVA fiber was used in this study (Figure 3.3).



Figure 3.3 PVA Fiber used in the production of ECC

The use of PVA fiber was decided based on and PVA-ECC represents the most practical ECC used in the field (Li et al., 2001; Kunieda and Rokugo, 2006) at the present. PVA fibers have attracted most attention due to the outstanding composite performance and economics consideration. The dimensions of the PVA fiber are 8 mm in length and 39 μm in diameter. The nominal tensile strength of the fiber is

1620 MPa and the density of the fiber is 1300 kg/m³. The mechanical and geometric properties of PVA fibers are summarized in Table 3.2. The surface of PVA fibers were coated with hydrophobic oiling agent (1.2% by weight) for the purpose of reducing the interfacial bonding strength between fiber and matrix. To account for material inhomogeneity, a fiber content of 2% by volume in excess of the calculated critical fiber content has been typically used in the mix design. Decision on the usage of fiber was made according to ECCs micromechanical material design and it was experimentally proved that good properties are obtained as a result (Li et al., 2001; Kong et al., 2003a).

Table 3.2 Mechanic and Geometric Properties of PVA Fibers

Fiber Type	Nominal Strength (MPa)	Apparent Strength (MPa)	Diameter (μm)	Length (mm)	Young Modulus (GPa)	Strain (%)	Specific Weight kg/ m³
PVA	1620	1092	39	8	42.8	6.0	1300

3.2 ECC Mixing and Specimen Preparation

An experimental program was designed to investigate the self-healing capability of ECC mixtures based on mineral admixture types, mechanical pre-loading deformation levels and curing regimes. For this purpose, three different ECC mixtures were prepared; namely F_ECC, C_ECC and S_ECC with Class-F fly ash, Class-C fly ash and slag, respectively. Specimens with water to cementitious material ratio (W/CM) of 0.27 and mineral admixture to portland cement (FA/PC or S/PC) ratio of 2.2 were produced. The proportions of three mixtures were presented in Table 3.3.

Table 3.3 ECC mixture proportions containing fly ash and slag, by weight

Mix ID.	Cement	W/CM	Aggregate/Binder ratio	FA/PC	S/PC	PVA, by volume (%)	HRWR (kg/m³)
F_ECC	1	0.27	0.36	2.2	-	2	3.8
C_ECC	1	0.27	0.36	2.2	-	2	4.2
S_ECC	1	0.27	0.36	-	2.2	2	4.5

To obtain approximately similar workability and uniform dispersion of fibers, the HRWR content was varied from mix to mix. As seen from Table 3.3, the ECC mixture incorporating slag had the highest HRWR demand compared with the specimens casted with FA. It is likely to say that due to smooth surface characteristics and spherical shape of FA particles similar workability properties were obtained with lower HRWR amount compared with slag particles at the same W/CM ratio (Figure 3.2).



Mixing of solid ingredients



Water addition



HRWR addition



Fiber addition

Figure 3.4 Production of ECC by using Hobart Type mixer

In this study, a Hobart type mixer (Figure 3.4) with 20-liter capacity was used in preparing all ECC mixtures. Solid ingredients, including cement, mineral admixture (FA or S), and aggregate, were first mixed at 100 rpm for a minute. Water and HRWR admixture were then added into the dry mixture and mixed at 150 rpm for one minute and then at 300 rpm for another two minutes to produce a consistent and uniform ECC matrix (without PVA fiber). PVA fiber was added in last and mixed at 150 rpm for an additional three minutes.

To determine the splitting tensile strength and chloride ion permeability behavior of the ECC mixtures, $\text{Ø}100 \times 200$ mm cylinder specimens were prepared. The molds were removed at the end of 24 h and the cylinder specimens were moved inside the lime saturated water at 23 ± 2 °C for 60 days. The submersion of specimens in water for a long time period guarantees further advances in both hydration processes and pozzolanic activity. For the flexural and compressive strengths characterizations of the ECC mixtures, $360 \times 50 \times 75$ mm prism specimens and 50 mm-cube specimens were prepared, respectively. All specimens removed from the molds after 24 h, and moisture cured in plastic bags at $95 \pm 5\%$ RH, 23 °C for 7 days. The specimens were then air cured in laboratory at $50 \pm 5\%$ RH, 23 °C until the age of testing.



Figure 3.5 Curing of ECC specimens after production of them (a) Cube and prism specimens, (b) Cylindrical specimens

3.3 Pre-cracking and Self-Healing Evaluation Methods

At the end of 60 days of water immersion, all cylindrical specimens were evenly divided into three 50 mm pieces with the help of diamond blade saw. Since ratio of W/CM is fixed, curing conditions and the testing age are same for all mixtures, the effect of SCM on test results is dominant. To derive the splitting tensile stress-deflection relation of ECC mixtures, at the age of 60 days, four cylindrical specimens ($\text{Ø}100 \times 50$ mm) from each mixture were loaded up to failure. Plywood strips were placed between the loading plates and the specimen to prevent the specimens from crushing at the loading points (Figure 3.6).

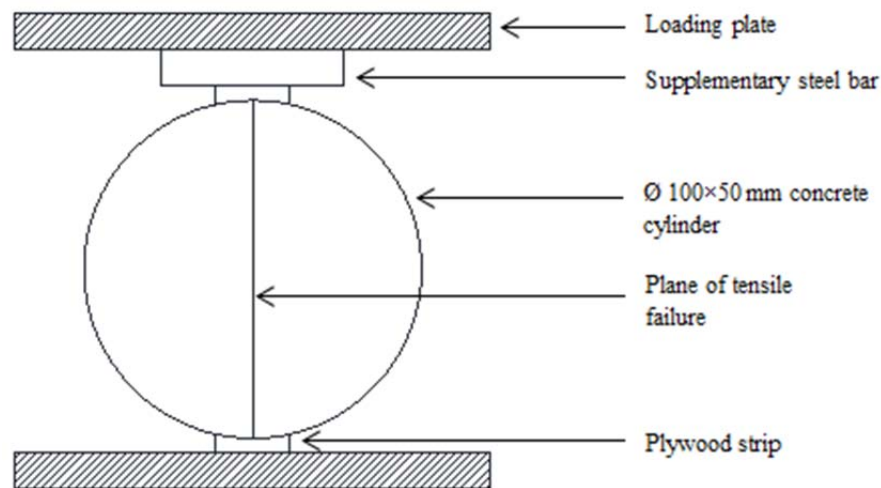


Figure 3.6 Splitting tensile strength test setup

Both the ultimate splitting load carrying capacities and ultimate splitting deformation capacities of ECC mixtures with different SCMs were close each other. Therefore, it has been decided to pre-crack the cylindrical specimens by loading up to 1.00 mm, 1.25 mm and up to failure deformation levels under splitting tensile loading at a loading rate of 0.005 mm/s to obtain different levels of microcrack damage before being exposed to different curing regimes. After reaching the predetermined deformation levels, the specimens were unloaded, and removed from the universal test machine to prepare for exposure to different environments. Upon unloading, crack characteristics were analyzed using an optical microscope with the maximum enlargement of 125X. Preloaded specimens up to failure showed localized large cracks with crack width of more than 200 μm . On the other hand, due to the high

tensile ductility of ECC, the specimens preloaded to a deformation level of up to 1.25 mm remain in the deformation-hardening stage, displaying microcrack damage but no localized large cracks. For the specimens not loaded up to failure, as a result of split tensile loading to ECC cylinder specimens, in addition to cracks with the widths between 50 and 140 μm , many cracks with width less than 20 μm were also observed. Among the ECC mixtures studied, S_ECC samples had a wider average crack width compared to the FA-ECC (F_ECC and C_ECC) samples.

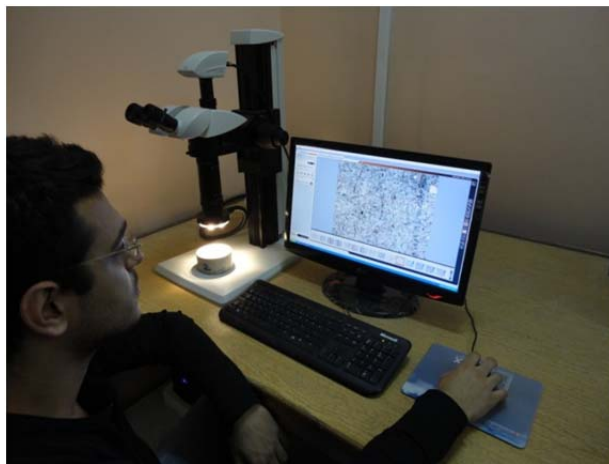


Figure 3.7 Control of crack widths of specimens tested by splitting tensile test

At the age of 60 days, the rapid chloride permeability testing (RCPT), based on the ASTM C1202, was conducted on the pre-cracked and virgin ECC specimens to determine whether microcracking due to mechanical pre-loading affects chloride ion penetration resistance or not. The RCPT is virtually a measurement of electrical conductivity of concrete—an indirect measure of chloride penetrability (Shi, 2004) which depends on both the pore structure characteristics and pore solution chemistry of concrete. However, it has been stressed by (Misra et al., 1994) that chloride permeability as measured from RCPT can be used for quality control of concrete. As more chloride ions migrate into the ECC specimen, more current can pass through, and the total charge passed during 6 h increases. A high value for total charge passed indicates that the ECC is highly penetrable.

Another method used to assess autogenous healing in this study incorporated a scanning electron microscope (SEM) to observe self-healing products. X-ray diffraction (XRD) analysis technique was also used to chemically analyze healing

products. These techniques are particularly useful in verifying the chemical makeup of self-healing compounds, essential in identifying the chemical precursors to self-healing and ensuring their presence within the composite.

3.4 Environmental Conditioning

The pre-loaded ECC disc specimens together with some pristine (uncracked) disc specimens were subjected to different exposure conditions at room temperature for 30 and 60 days before testing to determine how much healing was occurred in terms of rapid chloride permeability. Three different conditioning regimes were used to simulate different environmental exposures and to investigate their influences on the rapid chloride ion permeability of ECC mixtures at different ages by using four disc specimens at each age. Therefore, the self-healing effect was deduced from the change in RCPT results. Three different conditioning regimes are detailed below.

- The first curing regime (CA – continuous air) considered direct exposure to laboratory air at 23 °C, 50±5% RH until the predetermined testing ages. This conditioning is used as the reference curing regime.
- The second curing regime (CW – continuous wet) consisted of submersion in water at 23 °C until the predetermined testing ages. This regime is used to simulate underwater structures.
- The third curing regime (F/T – freeze/thaw cycle) considered ASTM C666 Procedure-A (1997) conditions: the specimens were kept in fully saturated condition with temperature cycling between –17.8 and 4.4 °C, each cycle being around 5 h. Each complete 5 cycle therefore represents one day of exposure. The resulting data is important in view of the growing use of ECC, especially for highway pavements, airport pavements, and bridge decks in cold climate regions.

3.5 Test Procedure

3.5.1 Compressive Strength

Nine cubic samples (3 specimens for each of age) of 50 mm were cast from each ECC mixture. The compression test was carried out on the cubic specimens by using

a 3000 kN capacity testing machine in accordance with ASTM C39 (2003) (Figure 3.8). ECC cubic samples were tested for compressive strength measurement at the age of 7, 28 and 60 days.



Figure 3.8 Compression testing machine and cubic samples

3.5.2 Flexural Performance

To measure the flexural performance of ECC mixture, twelve prismatic samples (4 specimens for each age of testing) having dimensions of 360x75x50 mm were cast from each produced ECC mixture. ECC prisms were first cleaned, and then flexural strength under four-point test was performed by using universal testing system (Figure 3.9).

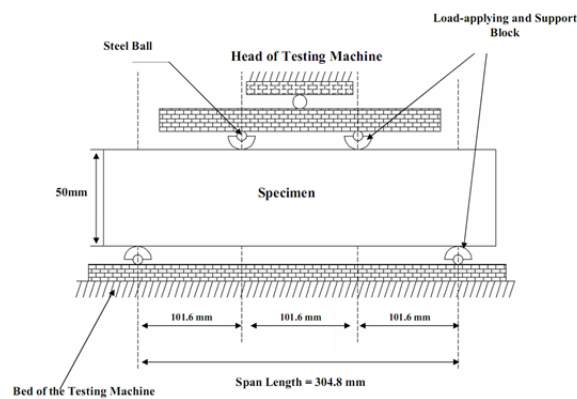


Figure 3.9 Four-point bending test setup

Four point bending test was performed on a closed-loop controlled material test system at a loading rate of 0.005 mm/s. The capacity of the loading frame was 100 kN (Figure 3.10). A four point bending loading fixture was developed to eliminate extraneous deformations such as support settlements and specimen rotations. The span length of flexural loading was 304 mm with a 101 mm center span length. During the flexural tests, the load and mid-span deflection were recorded on a computerized data recording system. Linear variable displacement transducer (LVDT) was fixed on the test set-up to measure the flexural deflection of the specimens.



Figure 3.10 Four-point flexural strength test

3.5.3 Freezing and Thawing Test

Six air cured cylindrical specimen from each mixture were exposed to 150 and 300 F/T cycles in accordance with ASTM C666 Procedure A. Specimens were completely submerged in water while they were testing in the freeze/thaw machine (Figure 3.11). The F/T cycles consisted of alternately lowering the temperature of the specimens from 4.4 to -17.8 °C and raising it from -17.8 to 4.4 °C in 5 hours. Since each cycle was around 5 hours, it took 30 and 60 days for the F/T machine to be terminated. After the exposure, self-healing capability under F/T cycling damage on

pristine and mechanically preloaded ECC specimens was evaluated by means of RCPT changes.



Figure 3.11 Specimens in freezing and thawing machine

3.5.4 Rapid Chloride Permeability Test (RCPT)

Rapid chloride permeability test (RCPT) was performed by monitoring the amount of electrical current that passed through a sample 50 mm thick by 100 mm in diameter in 6 hours, which standardized with ASTM C 1202. This sample was cut as a slice of a 100x200 mm cylinder. A voltage of 60V DC was maintained across the ends of the sample throughout the test. One lead was immersed in a 3.0% salt (NaCl) solution and the other in a 0.3 M sodium hydroxide (NaOH) solution. Based on the charge that passed through the sample, a qualitative rating was made of the concrete's permeability (Figure 3.12).



Figure 3.12 Rapid chloride permeability test (RCPT) setup

CHAPTER IV

RESULTS AND DISCUSSIONS

4.1 Compressive Strength

At the ages of 7, 28 and 60 days, compressive strength tests for cubic specimens were applied following ASTM C39 (2003) procedures. Table 4.1 tabulates the average of compressive strength results as determined from at least three cubic specimens. As it is seen from Table 4.1, for the first 7 days of curing, strength gain in the specimens casted with slag (S_ECC) was significantly higher compared to the mixtures casted with fly ash (F_ECC and C_ECC) but between the ages of 28 days and 60 days high amount of strength gain was achieved by FA-ECC mixtures. This finding was partially a result of the advances in hydration and pozzolanic reactions of the slag due to its large specific surface area ($425 \text{ m}^2/\text{kg}$ surface area) compared to that of fly ashes ($269 \text{ m}^2/\text{kg}$ for Class-F FA and $306 \text{ m}^2/\text{kg}$ for Class-C FA). Due to the smaller average particle size of slag than that of cement, it can well fill the space among the cement grains (filler effect), improving the particle distribution of cementitious system, and forming dense microstructure. Moreover, high surface area of slag provides more nucleating sites and OH^- ions as well as alkalis into the pore fluid (Li and Zhao, 2003). At the ages of 7 days of curing, the compressive strength test results were similar for both F_ECC and C_ECC mixtures. However, the strength gain was more pronounced for C_ECC beyond 7 days of curing. This high strength should be correlated not only to the fineness but also to the self-cementitious activity of Class-C FA. The lime content of FA seems to contribute to the strength of ECC mixture. Nevertheless, all the mixtures exceeded the nominal compressive strength for normal concrete (30 MPa) at the age of 28 days which is an acceptable value for most of the construction practices.

Table 4.1 Basic mechanical properties of ECC mixtures

Mechanical Properties	F ECC			C ECC			S ECC		
	7 d.	28 d.	60 d.	7 d.	28 d.	60 d.	7 d.	28 d.	60 d.
Compressive Strength (MPa)	21.2	35.1	51.3	26.3	46.7	56.7	50.5	72.5	75.1
Flexural Strength (MPa)	6.7	9.6	10.6	6.8	8.7	10.5	9.6	12.0	12.2
Flexural Deformation (mm)	5.2	5.5	3.5	4.5	3.6	3.4	4.1	3.5	3.2
Splitting Tensile Strength (MPa)	-	-	4.1	-	-	4.3	-	-	5.8
Splitting Deformation (mm)	-	-	1.67	-	-	1.56	-	-	1.45

4.2 Flexural Performance

4.2.1 Flexural Strength (modulus of rupture – MOR)

The direct tensile test is considered to be the most accurate method to confirm the strain-hardening behavior of a composite, as quasi-brittle fiber reinforced composites can potentially show apparent strain-hardening behavior under flexural loading, depending on the specimen geometry. However, previous studies demonstrate that deflection capacity under bending can be correlated with the tensile strain capacity when the material is truly strain hardening (Qian and Li, 2008). Therefore, in this study, it was decided to use the four-point bending test to investigate the flexural strength and ductility of ECC mixtures.

During the four-point bending test, in all ECC specimens, the first crack was observed at the tensile face in the mid-span. As flexural stress increased, multiple cracks with small spacing and tight widths developed and propagated from the first cracking point. When the fiber bridging strength is reached for one of the microcracks, bending failure resulting in localized deformation occurred at that part of ECC specimen. As the modulus of rupture (MOR) was approached, one of the cracks inside the mid-span started to widen leading to complete failure. The test results in terms of flexural strength (MOR) and ultimate mid-span deflection at the peak stress at the end of 7, 28 and 60 days are displayed in Table 4.1. The flexural performances of ECC mixtures were calculated by averaging the results of four four-point bending measurements. It is important to note that the coefficient of variations

of the flexural strength test results within each mix design is lower than 10%. MOR values varied from 6.7 to 9.6 MPa showing that increase in the values of flexural strength of S_ECC was not that of drastic compared to the values of F_ECC and C_ECC for the first seven days as in the compressive strength test results. Moreover, for all specimens, no significant flexural strength gain was observed beyond the age of 7 days. The most probable reason for this trend may be attributed to the fact that flexural strength is governed by more complex material properties, such as tensile first cracking strength, ultimate tensile strength and tensile strain capacity, particularly in the case of strain hardening cementitious materials (Zhou et al., 2009).

4.2.2 Mid-span Beam Deflection

Ultimate mid-span deflection capacity, which reflects the material ductility, of the mixtures ranged between the values of 4.1 and 5.2 mm for the first 7 days. From 7 days to 60 days, for all mixtures, there is a slight decrease due to the continuous evolution of fiber/matrix interface properties. Among all the supplementary cementitious materials, F_ECC showed the highest deflection capacity, therefore ductility, at all ages (Table 4.1). The increased ductility can possibly be caused by the lower fracture toughness, bond strength and friction between F_ECC specimens compared with S_ECC. The microstructural studies provide some assistance in evaluating the differences in macroscopic behavior between F_ECC and S_ECC. In Figure 4.1 SEM observations of F_ECC and S_ECC specimens were displayed.

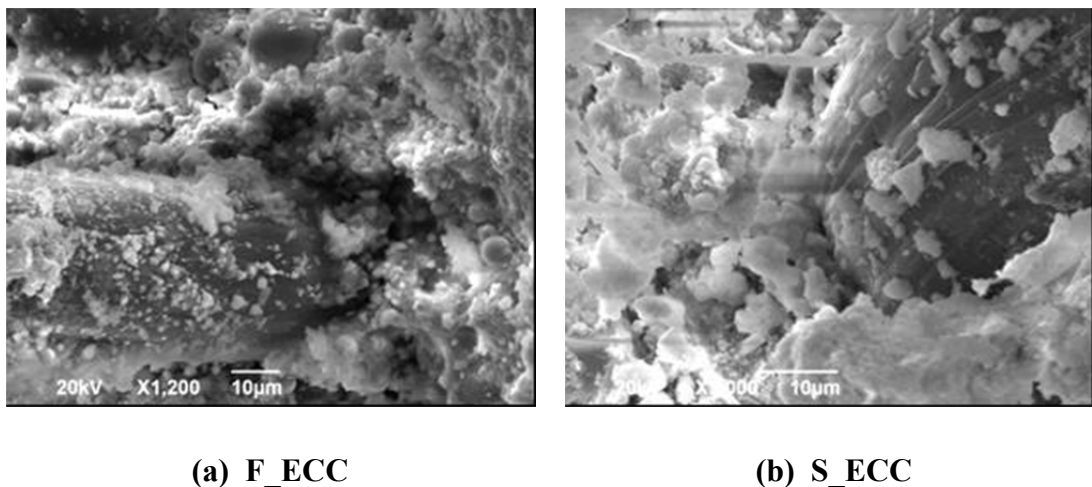


Figure 4.1 SEM image from the fractured surface

With the incorporation of slag, almost no unhydrated particles were observed. The increase in fiber/matrix frictional bond strength with an addition of slag was also verified with SEM image observations (Figure 4.1), which may be detrimental to achieving sufficient multiple cracking and strain-hardening behavior. Comparing Figure 4.1(a) with Figure 4.2(b), the fiber surfaces in S_ECC have more attached matrix material compared to F_ECC. For a fiber to be pulled out of the S_ECC matrix, de-bonding at the fiber-interface or fracture of the hydrate product is required to overcome interlocking of the hydrate product (Gao and Van Zijl, 2004). Therefore, the improvement in the mid-span beam deflection capacity with the use of Class-F FA can be attributed to the fact that the addition of Class-F FA has a tendency to reduce PVA fiber/matrix interface chemical bond and matrix toughness while increasing the interface frictional bond, in favor of attaining high tensile strain capacity (Wang and Li, 2007). In the case of C_ECC specimens, although it is not sure, the overall decrease in the mid-span beam deflection capacity might be associated with higher lime content which in turn causes enhanced fracture toughness, bond strength and the chemical bond between mortar matrix and fibers as in S_ECC specimens.

4.3 Rapid Chloride Permeability Test

4.3.1 Unhealed Specimens

The results of chloride permeability tests for each ECC mixture were demonstrated in Table 4.2. Specimens were tested at the age of 60 days to fulfill the requirements needed for more mature paste, and not to have contradictory results due to different characteristics of SCMs. As explained in previous sections, specimens were divided into three categories as preloaded to 0 mm (pristine), 1.00 mm and 1.25 mm deformation levels. Additionally, for the specimens exposed to CW curing regime, four more disc specimen was loaded up to failure at the ages of 60 days for comparison. RCPT results were recorded in coulombs at the ages of 60, 60+30 and 60+60 days, respectively.

Table 4.2 Rapid chloride permeability test results of ECC specimens

Preloading deformation level	60 day	60+30 day			60+60 day			
	CW	CW	F/T	AC	CW	F/T	AC	
F_ECC	0 mm	3867	1582	3880	2886	703	4267	1892
	1.00 mm	4358	1691	4339	3111	817	5291	2285
	1.25 mm	4964	1757	4850	3627	1104	5946	2608
	up to failure	6767	2172	-	-	1242	-	-
C_ECC	0 mm	1787	480	1534	715	161	1953	432
	1.00 mm	2066	531	1760	931	255	2226	570
	1.25 mm	2214	648	1927	1194	312	2339	619
	up to failure	2537	882	-	-	370	-	-
S_ECC	0 mm	468	284	344	329	245	378	254
	1.00 mm	764	315	527	462	274	614	373
	1.25 mm	1027	372	736	651	317	833	499
	up to failure	1371	530	-	-	427	-	-

As seen from Table 4.2, after 60 days of moist curing exposure S_ECC exhibited the lowest charge (468 Coulomb), then high-lime FA (1787 Coulomb), and low-lime FA the highest (3867 Coulomb). It, therefore, appears that the FA-ECC mixtures (F_ECC and C_ECC) were more permeable than the S_ECC mixture in accordance with RCPT results. The permeability difference can be discussed in related to SCM particle size, modification of pore size distribution due to pozzolanic and cementitious reaction and pore solution chemistry or electrical conductivity changes. The following facts are taken into consideration for the evaluation of permeability of different SCMs: (1) Class-F FA has a much coarser particle size than Class-C FA (Figure 1); (2) Slag has the finest particle size and (3) In related to available Na₂O equivalent alkali percentage by ASTM C33, Class-F FA 2.02, Class-C FA 4.45 and slag 0.94. Because slag has the finest particle size and lowest available alkali content, S_ECC mix has the lowest permeability among ECC mixtures. Class-C FA has higher equivalent alkali content than Class-F FA but finer particle size. This suggests that pore size distribution may be more related to chloride penetrability and thus the effect of Class-C FA replacement on chloride penetrability is due to a decrease in the pore size opening.

To investigate the effect of pore structure on ECCs' chloride permeability, the porosity and pore size distribution study was also carried out with mercury intrusion porosimetry (MIP) testing. The cumulative intruded pore volume curves for ECC

mixtures with different SCMs, obtained from MIP, are provided in Figure 4.2-a. This figure indicates that compared to S_ECC mixture, the total intruded volume of mercury per gram of the sample increases with the use of FA in ECC production. This increasing effect is, especially, more pronounced with the use of Class-F FA. It has been suggested that since different pore size affect different properties, the pore size distribution, not the total capillary porosity, is a better criterion for evaluating the impermeability characteristics of a hydrated cement paste. Macropillary voids larger than 50 nm are generally accepted to be more influential in determining the impermeability characteristics of hydrated cement-based materials (Mehta and Monteiro, 2006). Figure 4.2-b shows the normalized volumes of mercury intrusion in a specified range of pores (greater than 50 nm and 4–50 nm) for ECC mixtures. Analysis of the pore size distribution data shows that a similar trend of pore size distribution can be observed in S_ECC and C_ECC mixtures, and F_ECC has a significantly higher proportion of pore sizes within the macropores limits than C_ECC and S_ECC mixtures, as shown in Figure 4.2-b. The proportion of pores within the macropores classification ranges from 52.9% for F_ECC compared with 37.5% for C_ECC and 32.7% for S_ECC. The higher total volume of macropores in F_ECC could explain the higher magnitude of chloride permeability of pristine F_ECC specimens at the age of 60 days.

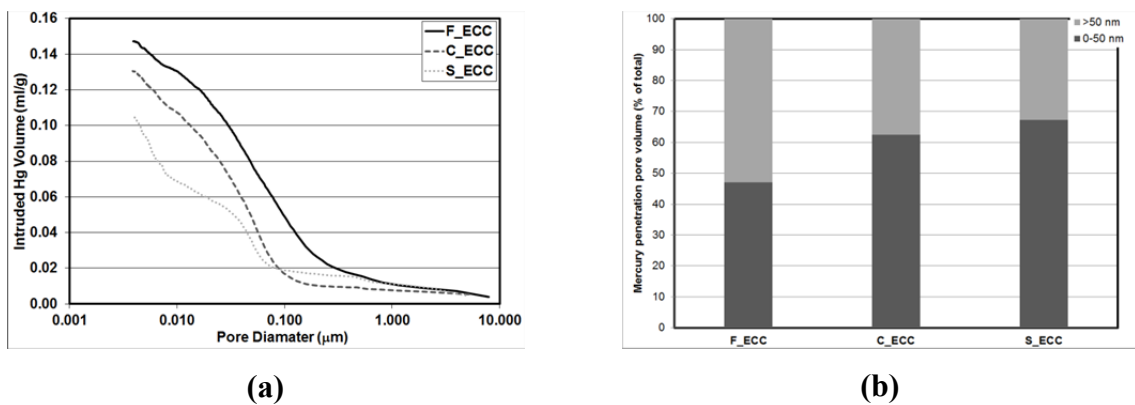


Figure 4.2 Changes in pore size distribution of ECC mixtures

This test result does not agree with the previous studies (Şahmaran et al., 2007; Şahmaran and Li, 2009a) which found that use of SCMs, especially FA, inhibits the ingress of chloride. Figure 4.3 displays that, the microstructure changed greatly with the incorporation of high volume Class-F FA and significant amount of FA particles

without any chemical reaction could be observed in the matrix even after 60 days of CW curing, which relatively influences the intensity of matrix. However, this is not the case for Class-C FA and slag; the matrix microstructure changed greatly, with the incorporation of Class-C FA slight and with the incorporation of slag and almost none unhydrated particles could be observed showing that the material is less penetrable. This result is in agreement with the widely acknowledged fact that FA (especially Class-F FA) content beyond 30-40% does not participate in the hydration process thus delays the hydration process (Gao and Van Zijl, 2004).

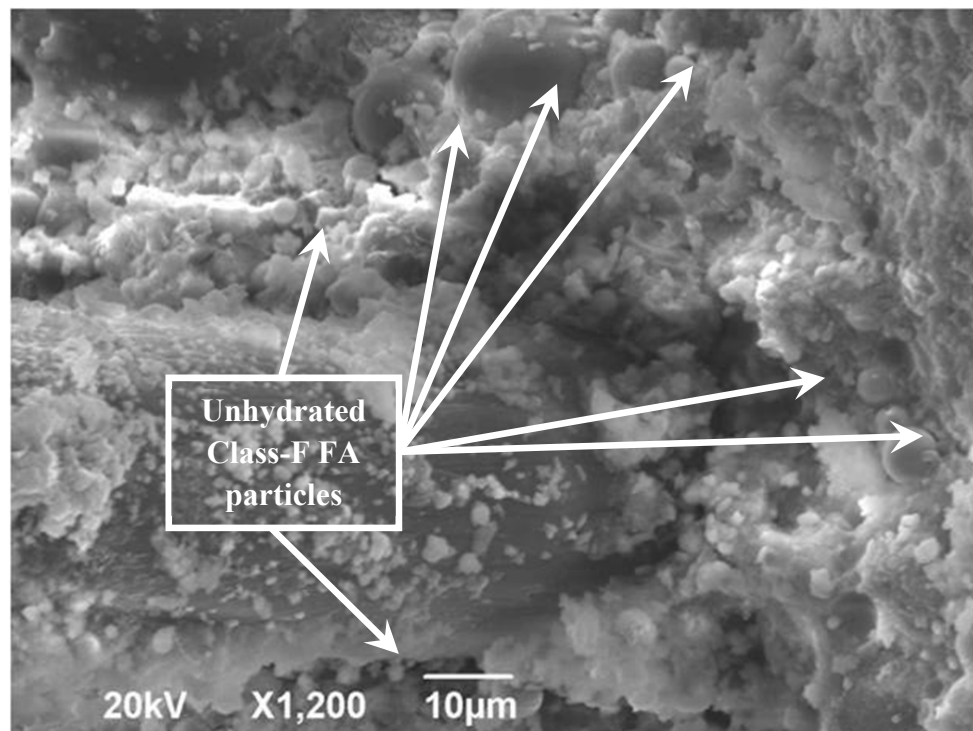


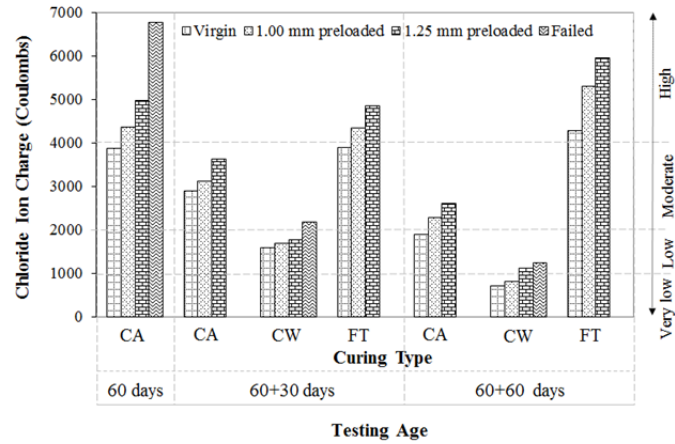
Figure 4.3 SEM observations of F_ECC mixture at 60 days of age

In HVFA ECC, however, secondary hydration of FA may only reach a very limited reaction degree because the FA content is relatively high in proportion to cement, and it may remain in the system as fillers even after a long time of curing. The benefits of a higher FA content are expected to manifest at later ages with the continuous supply of moisture and presence of CH in the hydrated matrix (Şahmaran et al., 2007).

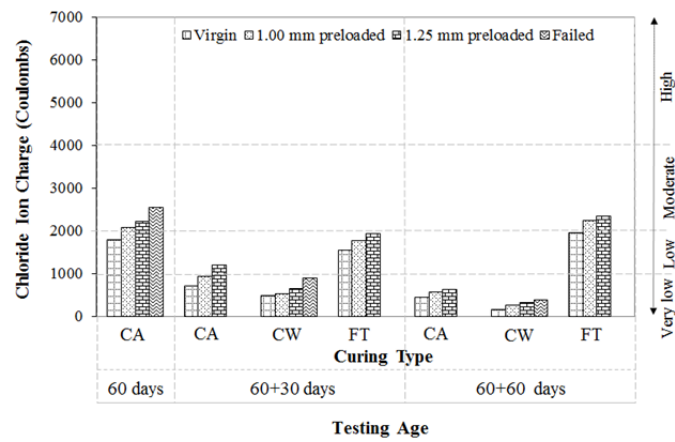
Chloride ion permeability test results of the preloaded specimens for ECC mixtures at 60 days are presented in Table 4.2 and Figure 4.4. The test results are expressed in terms of the total electrical charge in coulombs, which provides an indirect measure

of the resistance of precracked ECC specimens to chloride ion penetration according to the ASTM C1202. The classification ranges given in the ASTM C1202 are also illustrated graphically in Figure 4.4 by horizontal gridlines. As mentioned earlier, maximum splitting tensile deformation capacities of all ECC mixtures at 60 days was around 1.5 mm (Table 4.1). Specimens were, therefore, preloaded to deformation levels of 1.00 and 1.25 mm and up to failure. After unloading, multiple microcracks with a small average crack width and fine crack spacing were observed on all specimens. The measured average crack width is about 110 μm for S_ECC mixture, 65 μm for C_ECC mixture and 50 μm for F_ECC mixtures at 60 days age. Increasing the preloading deformation level leads to higher number of cracks, and so as the number of cracks increases. As these specimens were tested right after the release of pre-loading at the ages of 60 days, they had no time to undergo any crack healing. Properties of pristine specimens (preloading deformation level of 0 mm) are also shown in this figure. In literature, although the many researchers (Lepech and Li, 2009) argued that the permeation of concretes, which has crack width less than 100 μm generally behave like sound concrete, as seen from the figure, the presence of microcracking in ECC significantly alters the chloride ion transport properties measured as a function of the pre-loading deformation level. The chloride ion permeability rate as measured by RCPT increases with the number of microcracks associated with a particular preloading deformation level. In particular, for the highly damaged ECC specimens (loaded ≥ 1.25 mm deformation level), the measured chloride ion permeability rate was very fast thereby implying that microcracks induced by mechanical loading facilitated the chloride ion ingress in ECC. However, the increase was low for S_ECC specimens, and even for specimens loaded up to failure, S_ECC mixture exhibited high resistance (low penetration class according to ASTM C1202) to chloride ion penetration with the total charge exceeding 1371 coulombs in average for the failed specimen at the age of 60 days. On the other hand, use of FA in ECC production reduces the resistance to chloride-ion penetration of preloaded ECC specimens. This effect is more negatively influenced with the use of Class-F FA. At all stages, precracked F_ECC specimens were several times more conductive than those of C_ECC and S_ECC specimens. This may be attributed to the fact that the use of FA, especially Class-F FA, caused a reduction in the strength capacity and a weaker interfacial transition zone at the age of the preloading. Therefore, it could be stated that the properties of newly damaged F_ECC specimens

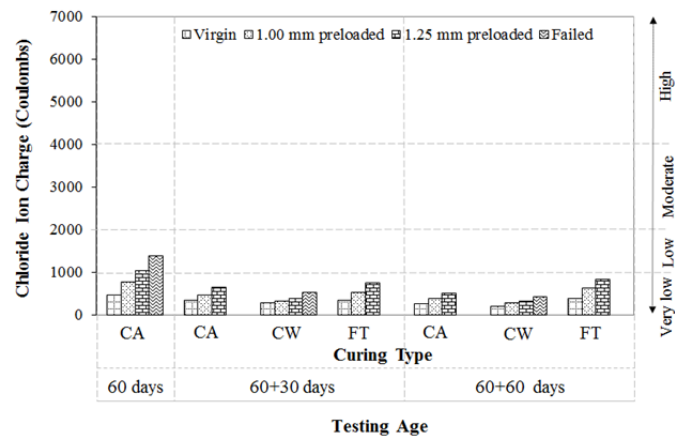
is more affected from the mechanical pre-loading than the C_ECC and S_ECC specimens.



(a) F ECC



(b) C ECC



(c) S_ECC

Figure 4.4 Chloride ion permeability values of the ECC mixtures under different curing conditions and testing ages

4.3.2 Effects of Self-Healing

Chloride ion permeability values in terms of RCPT were measured before and after splitting tensile preloading for each environmental conditioning to determine the effect of type and chemical composition of SCMs on self-healing capability of composites. Figure 4.4 shows the changes in chloride ion permeability of the ECC mixtures that were exposed to different curing regimes up to 60 days, CA – continuous air, CW – continuous wet, and F/T – freeze/thaw cycle, at different ages, after an initial 60 days continuously wet curing and applied preloading deformation levels. Each data point given in Figure 4.4 is an average of at least four specimens. For the pristine specimens, when the test results after 60 days are considered (Figure 4.4), it could be seen that there is a steady reduction in the chloride ion penetration properties with time irrespective of the applied further curing conditions. For example, results obtained from pristine F_ECC specimens cured continuously in water for 60, 90 and 120 days were 3867, 1582 and 703 coulombs, respectively. This result shows that for the first further 30 days of moist curing 59%, and for another further 30 days of curing 56% refinement in chloride permeability was attained. These rates are 73% and 66% for C_ECC and 40% and 14% for S_ECC at stated ages of curing. The reason for FA-ECC mixtures to exhibit notable improvement in chloride ion permeability results of pristine specimens may be attributable to the higher amounts of unhydrated cementitious particles present in system (see Figure 4.3). However, the situation was not the same for S_ECC, because, highly reactive slag performed its cementing reactions at early ages leading to decreased pore size and densified matrix. It is important to note that, even though S_ECC did not exhibit remarkable improvement in chloride permeability with the further CW curing as in the FA-ECC mixtures, it still exhibited very high resistance (very low penetration class according to ASTM C1202) to chloride ion penetration with the total charge less than 500 Coulombs in average at all ages. As mentioned earlier, contrary to the expectance, the use of FA (especially Class-F FA) in ECC production increased the chloride ion permeability of the ECC at the 60 days as a result of inadequate curing period. However, as seen from Figure 4.4, with further 60 days continuous wet curing, part of unhydrated cementitious particles are hydrated, reduced pore sizes and densified the matrix and decreased the chloride ion permeability values of the FA-ECC specimens drastically.

Surprisingly, with the application of CA curing, significant amount of improvement in terms of RCPT results was observed for all ECC specimens. For example, the results of chloride ion permeability of pristine F_ECC specimens were 2886 and 1892 for 60+30 and 60+60 days of further CA curing; the results were 715 and 432 for C_ECC, and 329 and 254 for S_ECC pristine specimens, respectively. It is surprising to observe this amount of improvement in permeation properties in the case of CA curing since the hydration of cementitious materials will stop completely when the internal humidity in hardened cement paste falls below 80%. (Mindess et al., 2002). During air curing period, the water in the isolated pores of hardened ECC mixtures can be used for further hydration and pozzolanic reaction, which could be one of the main reasons of reduced chloride ion permeability of CA cured ECC specimens. The reduction in RCPT results might also be attributed to the change on the composition of the pore solution with time, which can influence the electrical conductivity, and therefore chloride permeability test value of air-cured ECC mixtures.

In Figure 4.5, percent variations in chloride ion permeability values of ECC mixtures due to the effects of curing regimes and testing ages were shown. In this figure all results at a particular age and deformation level are compared with those results of 60 days of age. It is clear from Figure 4.5 that, RCPT results for all ECC specimens decreased as curing time extended showing that significant amount of self-healing is attained, except for specimens exposed to F/T cycle. As it is seen from Figure 4.5, however, change in chloride ion charge-testing age slope was not that of explicit for CA curing as in the case of CW curing conditions. Therefore, the effect of moist curing is more pronounced on the chloride ion permeability results of especially preloaded specimens, suggesting that water is the important parameter for further hydration reaction and self-healing to take place. As seen from Figure 4.5, for CW curing, chloride ion charge-testing age slope variation of ECC mixtures was quite different for FA-ECC mixtures (F_ECC and C_ECC) and S_ECC mixture. In general, there was no meaningful variation in the chloride ion charge-testing age slope due to the applied preloading level; the decreasing trend was fairly similar for F_ECC and C_ECC specimens. For these mixtures the chloride ion penetration decreasing trend between the ages of 60 and 60+30 days was continuous and drastic without regard to the preloading deformation level. Between the ages 60+30 and

60+60 days, the amount of percent variations slightly decreased irrespective of curing conditions and pre-loading deformation levels exhibiting that improvement of matrix maturity was achieved for FA-ECC specimens with the further curing.

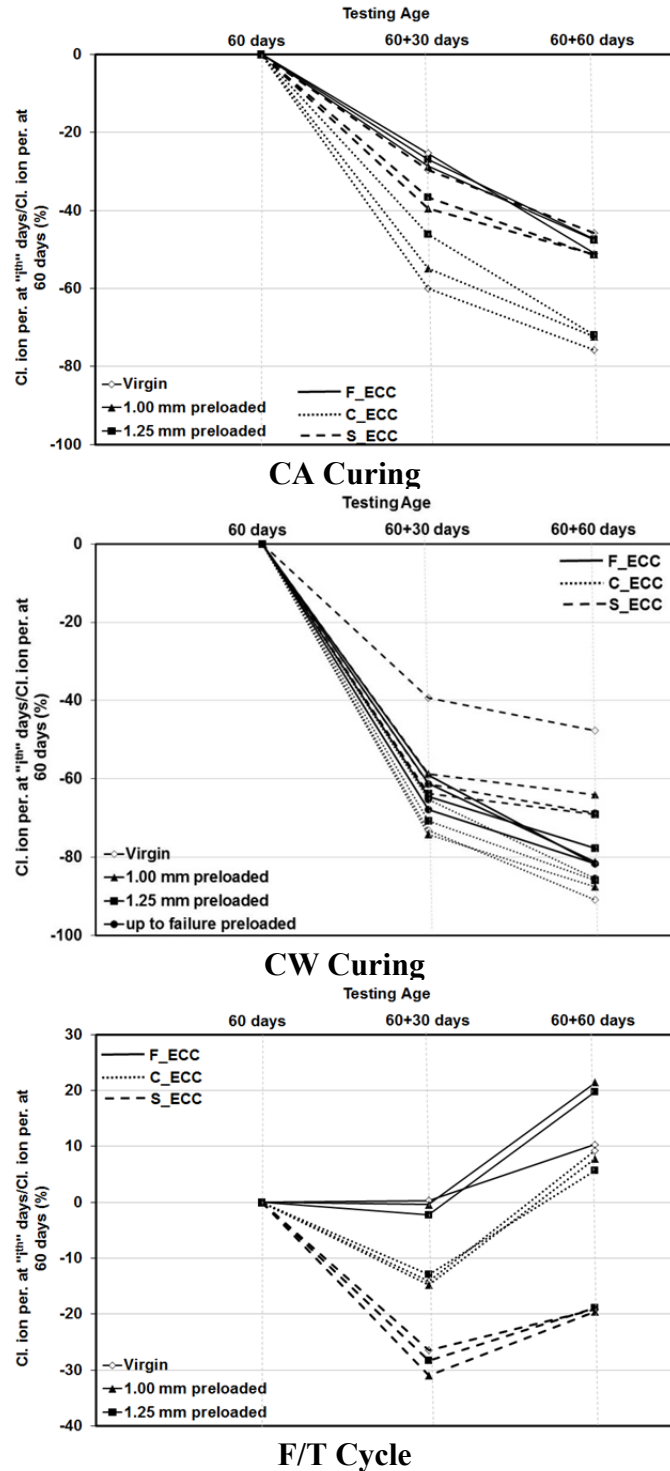


Figure 4.5 Percent variations in chloride ion permeability values of ECC mixtures due to the curing regimes and testing ages

Therefore, the results of FA-ECC mixtures indicate that longer curing age, especially with the presence of moisture, leads to higher crack self-healing ability. As we know, a large amount of unhydrated cementitious materials still existed inside of FA-ECC mixtures. With increasing in curing age after preloading, more and more resultants come from further hydration filled in the tiny cracks and resulted in self-repair of damaged concrete. However, the decrease trend in chloride ion permeability of S_ECC specimens became more evident with a month of further curing only when the preloading deformation was applied. Between 60+30 and 60+60 days, even under continuous water curing, the chloride ion charge-testing age slope of preloaded S_ECC specimens was very low and close to zero under the CW curing.

It therefore appears that the type and chemical composition of SCM used in the production of ECC significantly influences the self-healing rate and behavior cementitious composites. As will be confirmed by the observations of the microstructural investigations presented in the next section, compared with S_ECC, the chloride ion permeability of ECC mixtures containing FA was recovered due to the combined effects of the further hydration processes of unhydrated cement and SCM, and formation of calcium carbonate. Thus the chloride permeability was improved much higher for the precracked ECC mixtures containing FA and experienced longer curing age. On the other hand, the formation of calcium carbonate plays the decisive part in the self-healing of cracks in S_ECC mixture. The formation of calcium carbonate is affected by the leaching of the hardened matrix (Jooss, 2001) and from the test results of this study it is evident that the presence of cracks increased the leaching rate.

As another way of curing regime, specimens were subjected to F/T cycles. After subjected to the 150 and 300 F/T cycles, self-healing capability under F/T cycling damage on pristine and mechanically preloaded ECC specimens was evaluated by means of RCPT changes. Since, one day in F/T testing machine accounts for approximately 5 cycles, it can be stated that 150 and 300 F/T cycles took 30 and 60 days, respectively to terminate the F/T test for each ECC mixtures. In Figure 4.5, percent variations in chloride ion permeability values of ECC mixtures due to the effects of F/T cycles and testing ages were shown. As seen from Figure 5, a slight improvement in RCPT test result was observed in all ECC mixtures up to 150 F/T

cycles. The improvement rate is more obvious for S_ECC mixture. As a result of the formation of micro-cracks due to mechanical loading, therefore, unhydrated cementitious particles are easily exposed to the water during the thawing period, which leads to development of further hydration processes. Finally micro-cracks under conditions of a damp environment were partially healed by newly formed products.

On the other hand, at the end of 300 F/T cycles, all FA-ECC specimens regardless of preloading deformation level, showed an increase in RCPT values. The increase in chloride permeability results was more pronounced for the pre-loaded specimens. This trend is associated with the interconnection of already-existing microcracks with mechanically induced cracks leading to a further increase in overall crack size thus causing a more porous body which in turn triggers severe deterioration and increases RCPT results. The highest variation in RCPT results after frost action was observed on FA_ECC mixtures. Moreover F_ECC mixture has more deterioration than C_ECC mixture. It is, therefore, apparent from the data in Figure 4.5 that the frost deterioration after 300 F/T cycles overshadows the improvement in chloride ion transport properties of pristine and preloaded FA-ECC specimens. FA-ECC specimens also exhibited some surface scaling at the conclusion of the F/T cycling, and increased surface scaling was observed on the pre-loaded specimens (Figure 4.6).

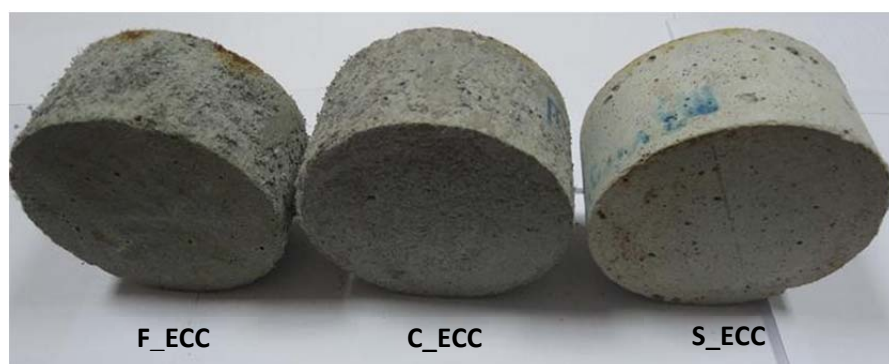


Figure 4.6 Surface conditions of ECC specimens after 300 F/T cycles

The scaling was, however, clearly confined to the surface layers of the test specimens, and had no effect on the integrity of the ECC mass. On the other hand,

compared to test result of 60 days of age, no increase in RCPT values and almost no surface scaling were observed on both pristine and preloaded S_ECC specimens after 300 cycles of F/T (Figure 4.6). This was probably due to the greater maturity of the S_ECC test specimens. When the strength properties before F/T cycling of the ECC mixtures are evaluated together (see Table 4.1), it can be concluded that there is a powerful relation among them. This result is in agreement with finding of the Sun et al (1999) in which different strength grades of concrete under the simultaneous action of load and F/T cycles were studied and concluded that at the same stress ratio, concrete of higher strength could undertake more F/T cycles, and the dynamic elastic modulus decreased more slowly with F/T cycles. With the effect of CW curing on further hydration processes for 60 days before being exposed to F/T cycles, the requirements needed for more mature paste were not achieved for FA-ECC mixtures, which caused to high chloride ion permeability results and significantly scaled composite surface. Therefore, FA-ECC needs more time (maturity) to develop beneficial characteristics in terms of frost durability.

4.4 Crack Characteristics and Microstructure

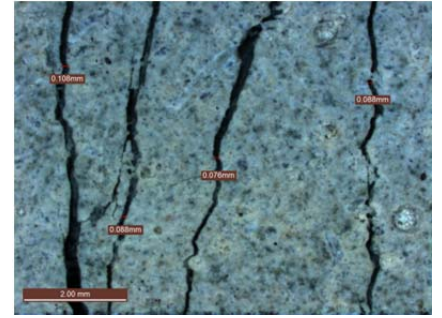
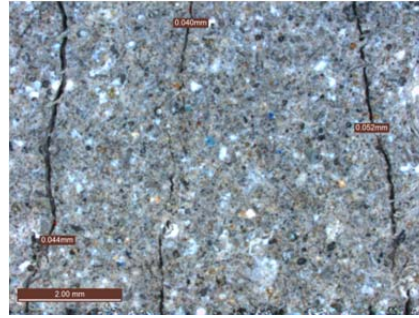
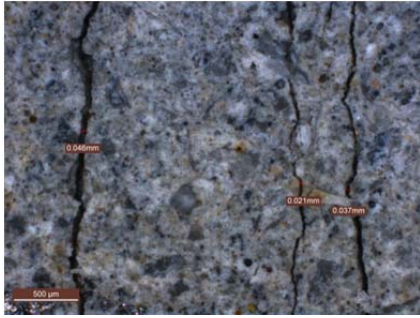
At the age of 60 days, except for the control specimens, all ECC cylinder specimens were pre-cracked by applying different splitting deformation levels using a splitting tensile test to obtain different crack frequencies. The application of different deformation levels resulted in a different number of cracks with different average crack width for each cylinder. All ECC specimens develop multiple micro-cracking as a result of the split preload. To account for the crack closure on unloading, all crack width measurements were conducted in the unloaded state. For each specimen, a line parallel to the longitudinal axis of the cylinder specimen was drawn and the number of cracks and crack width were measured along this line using an optical microscope. Crack characteristics of the ECC specimens were investigated for all curing conditions.

At the age of 60 days, as a result of splitting tensile loading, the FA-ECC samples had a tighter average crack width compared to the S_ECC samples. Figure 4.7(a) shows the crack damage on the surface of ECC specimens after being subjected to 1.25 mm splitting pre-loading deformation level.

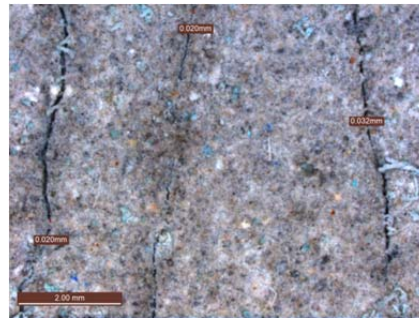
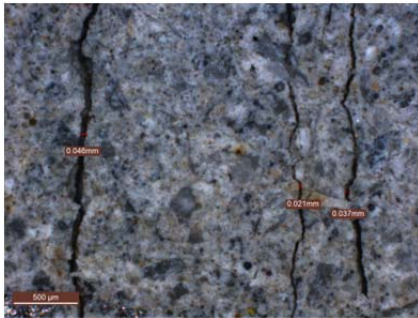
F_ECC

C_ECC

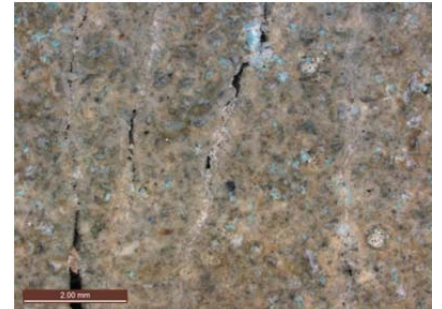
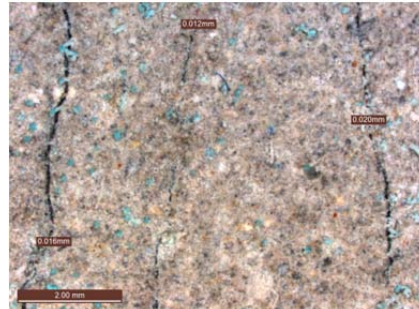
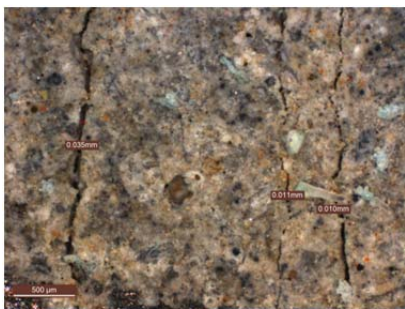
S_ECC



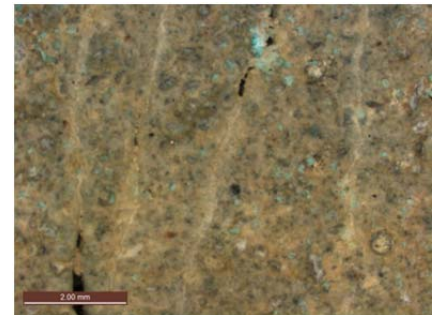
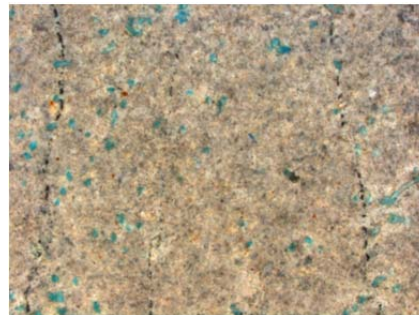
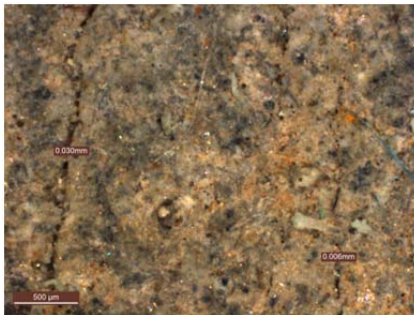
(a) Before self-healing (60 days of age)



(b) After 15 days of CW curing



(c) After 30 days of CW curing



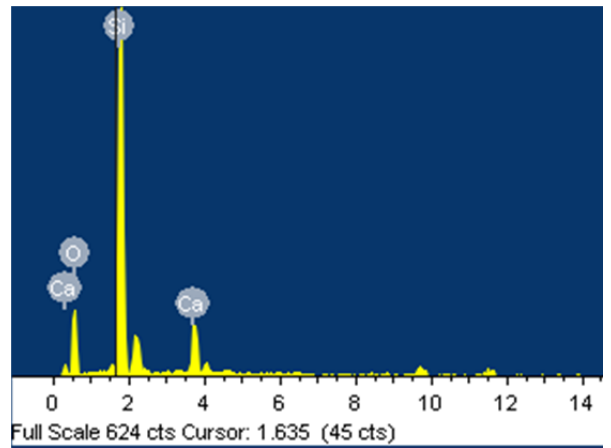
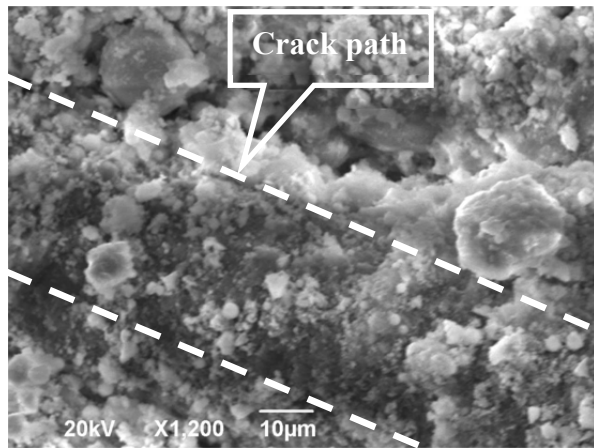
(d) After 60 days of CW curing

Figure 4.7 Self-healing in ECC microcracks before and after exposure to CW curing

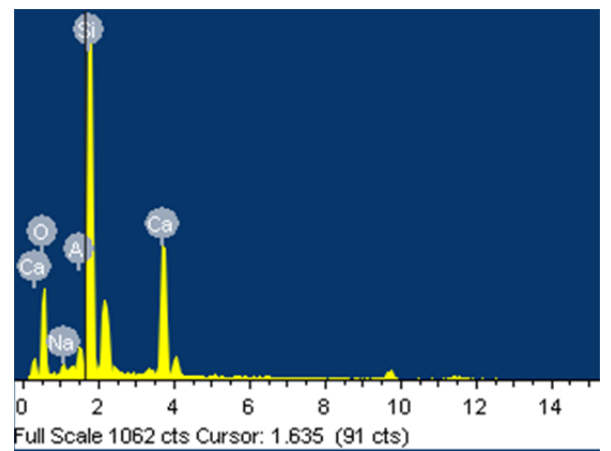
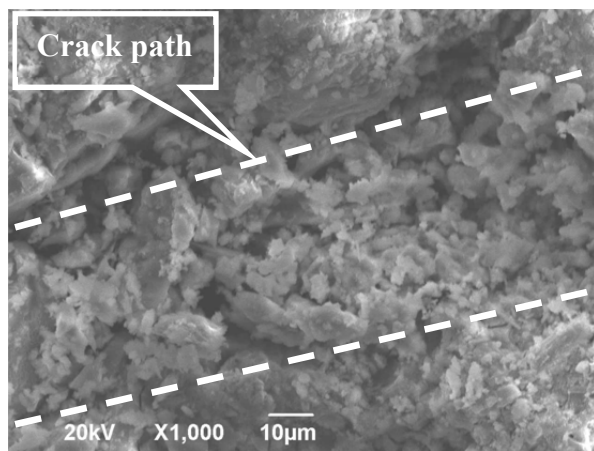
Figure 4.7(b-d) displays an image of the same location after CW curing. As seen from Figure 4.7, under the CW curing, self-healing ability was attained for all ECC mixtures up to certain degree depending on the crack width and type of SCMs. On the other hand, there was no or slight decrease in the average crack width value of the specimens that were exposed to the CA curing up to 60+60 days. Decrease in the crack width suggests that CW curing have greatly promoted the self-healing process and therefore enhanced the chloride ion transport properties after pre-cracking (see Figure 4.7).

Although FA-ECC samples have more unhydrated cementitious materials, and therefore, expectedly, a higher capacity for self-healing, more evident self-healing product was observed from S_ECC mixture. It can be roughly stated that, for the further 60 days CW curing after pre-cracking, critical crack widths for complete self-healing to take place were about 30 μm for F_ECC, 50 μm for C_ECC and slightly more than 100 μm for S_ECC. Even after 15 days CW curing, significant amount of self-healing product was observed within the cracks and near the crack faces on the S_ECC specimens' surface. These cracks of S_ECC specimens are covered by some white residue presumably due to the healing process under CW curing. On the contrast, there is almost none or slight such white residue exists on the FA-ECC samples.

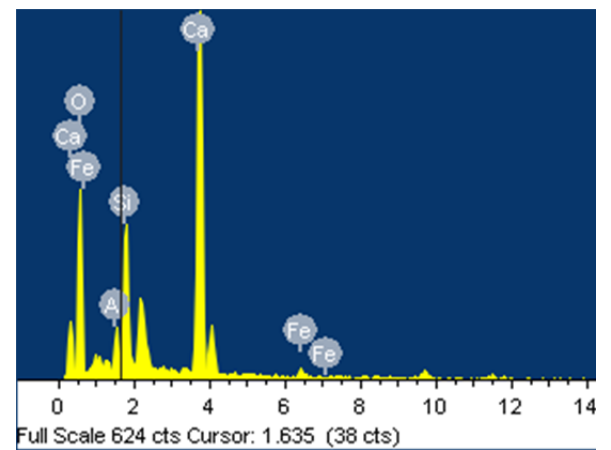
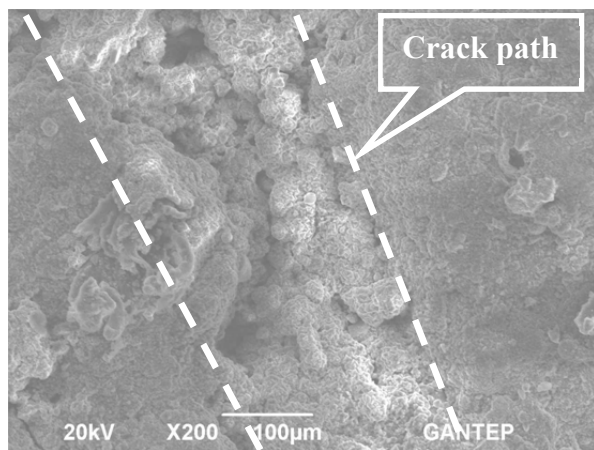
To characterize the self-healing process, healing products inside the microcrack were analyzed by SEM. Typical SEM pictures (with EDX detector) for ECC samples at the age of 60+60 days of CW curing are compared in Figure 4.8. As seen from the figure, the CW cured samples of ECC mixtures with different crack width appear to be completely healed. Surface chemical composition analysis via EDX reveals that the microcracks of FA-ECC samples with width of less than 50 μm were partly or completely filled with a mixture of C-S-H gels and calcite particles (Figure 4.8(a-b)), which are very likely due to the continuous hydration and pozzolanic reaction of SCM. On the other hand, the observations under SEM and XEDS confirmed that the microcracks with width of slightly wider than 100 μm in the S_ECC specimens cured under CW were healed with significant amount of calcium carbonate (Figure 8(c)).



a) F_ECC



b) C_ECC



c) S_ECC

Figure 4.8 SEM micrograph with EDX pattern of products in self-healed cracks

To complement the microscopy results, XRD analysis was also performed. A small amount of healing materials scratched from the precracked ECC samples was observed by XRD. X-ray diffractograms of ECC mixtures involved in this study

(Figure 4.9) show well-defined peaks. The diffractogram of pre-loaded FA-ECC specimen that underwent healing contained quartz (from fly ash and/or silica sand) and some calcite. The diffractogram of samples taken from pre-loaded C_ECC (Figure 4.9) appears similar to that of F_ECC (Figure 9), though the peaks related to calcite are slightly better defined (Figure 4.9). Although some quartz is still evident from diffractogram obtained from pre-loaded S_ECC specimens, the majority of peaks are related to calcite (Figure 4.9). Overall, these results indicate that calcite is the primary crystalline product involved in the healing process of S_ECC. To facilitate healing of the cracks and promote formation of calcium carbonate, Ca^{2+} from hydration products must leach out of the hardened matrix into cracks and react with carbon dioxide. Without the presence of water, this leaching process is not possible. Carbon dioxide in gaseous form only reacts with CH in sufficiently high relative humidity and over long time periods (Neville, 2002). Water or water curing also provide a much higher concentration of carbon dioxide, both as a dissolved gas and as a bicarbonate solution, than that of the laboratory air curing, where the amount of carbon dioxide is limited (Kenneth and Floyd, 1956). Continued hydration of unhydrated cement particles is also faster in water. Because of mentioned considerations, preloaded specimens, which were further cured under CW had healed itself better than those of exposed to further CA curing.

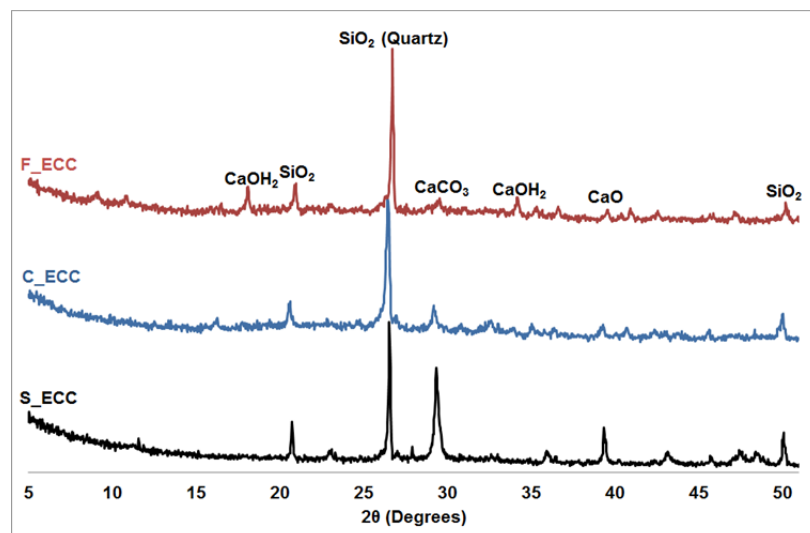


Figure 4.9 XRD patterns of self-healing products in ECC mixtures

The fast and high self-healing capability of pre-cracked S_ECC specimens might be correlated with the high pH value of pore solution. It is well-known that C-S-H gels

together with CH and alkalis (Na_2O and K_2O) present in the system dominate the chemical properties of aqueous phase in the cement paste and are responsible for high pH value of pore solution. Initially, with the dissolution of alkalis, pH value of more than 12 in the pore solution is easy to attain (Anstice et al., 2005). However, this hyper-alkaline stage is not long-lasting and with the further consumption of hydroxides in time, pH value is expected to decrease. The consumption of hydroxides which is associated with the pozzolanic capacity of SCMs is more understandable by controlling the main ingredients tabulated in Table 2. As it is seen from Table 3.1, amount of SiO_2 which is one of the main ingredients responsible for the pozzolanic activity is higher for FAs compared to slag. The amount of CaO that is mainly responsible for the cementing behavior, however, is higher for slag compared to FAs. Decrease in pH value which has a close relationship with the dissolution of carbonate species and final self-healing behavior in late age can be associated with the high amounts of SiO_2 that would lead to consumption of further CH in the case of C_ECC and F_ECC specimens (Edvardsen, 1999). Since, the amount of CH is expected to be high for S_ECC specimens due to low levels of SiO_2 amount in slag, it is likely to say that pH value were kept higher even at the late ages leading to higher rates of Ca^{2+} leaching from C-S-H gels which in turn triggers high levels of self-healing. Further investigations must be made to understand even more to see the rate of carbonation that would lead to significant amount of self-healing in the case of cementitious composites.

CHAPTER V

CONCLUSIONS

The self-healing behavior of a series of pre-cracked ECC incorporating different SCMs is investigated in this paper, focusing on the recovery of its chloride ion permeation properties. Three SCMs (Class-C and Class-F fly ashes and slag), selected to represent the wide range of composition of SCM, were used in the study. To generate microcracks, the splitting tensile preloading deformation levels were chosen as 1.00 mm, 1.25 mm and up to failure. The pre-determined deformation levels were introduced to ECC mixtures at the age of 60 days, and specimens were further exposed to CW, CA and cyclic F/T curing conditions up to 60+60 days. In order to observe the effects of different SCMs on the self-healing capability of ECC mixtures, RCPT and detailed microstructural analysis were conducted at the pre-specified days. From the results obtained, the following conclusions can be drawn:

1. Different from the water penetration properties of microcracked ECC specimen (Lepech and Li, 2009) the applied splitting tensile preloading affected the chloride ion penetration of the ECC specimens irrespective of the pre-loading deformation level. In particular, for the highly preloaded ECC specimens, the measured chloride ion permeability rate was very fast thereby implying that microcracks induced by mechanical loading facilitated the chloride ion ingress in ECC. However, compared to the FA-ECC specimens, the increase was low for S_ECC specimens, and even for specimens loaded up to failure, S_ECC mixture exhibited high resistance to chloride ion penetration.
2. Except for the specimens exposed to F/T cycle, RCPT results for all ECC specimens decreased as curing time extended showing that significant amount of self-healing is attained. The effect of CW curing is more pronounced on the chloride ion permeability results of especially for the preloaded specimens, suggesting that water is the important parameter for further hydration reaction and self-healing to occur.

3. At the end of 300 F/T cycles, all FA-ECC specimens regardless of preloading deformation level, showed an increase in RCPT values. The increase in chloride permeability results was more pronounced for the pre-loaded specimens. Moreover, compared to Class-C FA, the use of Class-F FA can further exacerbate the deterioration caused by F/T cycles. On the other hand, no increase in RCPT values were observed on both pristine and preloaded S_ECC specimens even after 300 cycles of F/T.

4. The microscopic observation of the pre-loaded ECC specimens showed that, self-healing was attained up to certain limits, regardless of the mixture type. However, the main restriction for an absolute self-healing to take was correlated back to the permissible crack widths. It was roughly found that F_ECC specimens could heal the cracks with the width of 30 μm . This value was around 50 μm for C_ECC and slightly above 100 μm for S_ECC specimens. Microstructural analysis also indicated that the main self-healing products are calcite and C-S-H gels, varying by SCM types used in ECC production. C-S-H and calcite are the main self-healing products for FA-ECC mixtures, and calcite is the main self-healing product for S_ECC mixture. The reason behind the significant amount of self-healing attainment of S_ECC specimens may be associated with the higher pH value of the pore solution that would favor the precipitation of calcite.

REFERENCES

ACI Committee 116R. (1994). Cement and concrete terminology. ACI manual of concrete practice.

ACI Committee 318R (2002). Building Code Requirements for Structural Concrete and Commentary. American Concrete Institute, Farmington Hills, Michigan, pp. 443.

ASTM Standard C618. (2003). Standard specification for coal fly ash and raw or calcined natural pozzolan for use in concrete. American society for testing and materials. West Conshohocken, PA, USA.

Aldea, C., Song, W., Popovics, J.S., Shah, S.P. (2000). Extent of healing of cracked normal strength concrete. *Journal of Materials in Civil Engineering.*, **12** 92-96.

Anstice, D., Page, C. and Page, M. (2005). The pore solution phase of carbonated cement pastes. *Journal of Cement and Concrete Research*, **35** 377–383.

ASTM C666-97. (1997). Standard test method for resistance of concrete to rapid freezing and thawing. American society for testing and materials. West Conshohocken, PA, USA.

ASTM Standard C1202. (1997). Standard test method for electrical indication of concrete's ability to resist chloride ion penetration. In: Annual book of ASTM standards, Philadelphia, PA, USA.

ASTM Standard C39. (2003). Standard test method for compressive strength of cylindrical concrete specimens. American society for testing and materials. West Conshohocken, PA, USA.

ASTM Standard C989. (2009). Standard specification for slag cement for use in concrete and mortars. American society for testing and materials. West Conshohocken, PA, USA.

Cernica, J.N. (1982). *Geotechnical Engineering*. Holt, Reinhart & Winston, New York, pp. 97-99.

Clear, C.A. (1985). The effects of autogenous healing upon the leakage of water through cracks in concrete. *Cement and Concrete Association, Wexham Springs*, p. **28**.

Cowie, J. and Glassert, F.P. (1992). The reaction between cement and natural water containing dissolved carbon dioxide. *Advanced Cement Research*, **14**(15) 119-34.

Edvardsen, C. (1999). Water permeability and autogenous healing of cracks in concrete. *ACI Materials Journal*, **96**, 448-454.

Gao, Song and Van Zijl, G.P.A.G. (2004). Tailoring ECC for commercial application. In: M. di Prisco, R. Felicetti and G.A. Plizzari, Editors, *Fibre-Reinforced Concretes (BEFIB'2004)*, *RILEM Pro039*, pp. 1391–1400.

Garrels, R. M., and Christ, C. L. (1965). *Solutions, Minerals, and Equilibria*. Harper and Row, New York.

Glasser, F.P. (1991). Chemical, Mineralogical, and Microstructural Changes Occuring in Hydrated Slag-Cement Blends. *Materials Science of Concrete II*, The American Ceramic Society, Inc., Loc., pp. 41-81.

Guppy, R. (1988). Autogenous Healing of Cracks in Concrete and Its Relevance to Radwaste Repositories. *Safety Studies*, Nirex Radioactive Waste Disposal (NSS/R105), Hardwell Laboratory, Ukaea.

Inaguma, H., Seki, M., Suka, K. and Rokugo, K. (2005). Experimental study on crack-bridging ability of ECC for repair under train loading. *Proc. Of Int'l Workshop on HPRCC in Structural Applications*, Honolulu, Hawaii, USA., pp. 499-508.

Jacobsen, S., Marchand, J. and Homain, H. (1995). SEM observations of the microstructure of frost deteriorated and self-healed concrete, *Cement and Concrete Research*, **25**, 1781-1790.

Jooss, M. (2001). Leaching of concrete under thermal influence, *Otto-Graf-Journal*, **12** 51–68.

- Kanda, T. and Li, V.C. (1999). A New Micromechanics Design Theory for Pseudo Strain Hardening Cementitious Composite. *ASCE Journal. of Engineering Mechanics*, **125** (4) 373-381.
- Kanda, T., Saito, T. and Sakata, N. (2003). Tensile and anti-spalling properties of direct sprayed ECC. *Advanced Concrete Technology*, **1**, 269-282.
- Kenneth, R.L. and Floyd, O.S. (1956) Autogenous healing of cement paste. *Journal of American Concrete Institute*, **27** 1083-1097.
- Kim, Y.Y., Kong, H.J. and Li, V.C. (2003). Design of Engineered Cementitious Composite (ECC) suitable for wet-mix shotcreting. *ACI Materials Journal*, **100**, 511-518.
- Kong, H.J., Bike, S. and Li, V.C. (2003a). Development of a Self-Consolidating Engineered Cementitious Composite Employing Electrosteric Dispersion/Stabilization. *Journal of Cement and Concrete Composites*, **25**, 301-309.
- Kosmatka, S.H. and Panarese, W.C. (1988). Design and control of concrete mixtures. Thirteenth ed. Portland Cement Association, Skokie, IL pp.205.
- Kunieda, M. and Rokugo, K. (2006). Recent Progress on HPFRCC in Japan. *Journal of Advanced Concrete Technology*, **4**, 19-33.
- Lepech, M. and Li, V.C. (2007). Large Scale Processing of Engineered Cementitious Composites. Accepted for publication in *ACI Materials Journal*, July 2007.
- Lepech, M.D. and Li, V.C. (2009). Water Permeability of Engineered Cementitious Composites. *Cement and Concrete Composites*, **31** 744–753.
- Li, G. and Zhao, X. (2003). Properties of concrete incorporating fly ash and ground granulated blast-furnace slag. *Journal of Cement and Concrete Research*, **25** (2003) 293–299.
- Li, V.C. and Leung, C.K.Y. (1992). Theory of steady state and multiple cracking of random discontinuous fiber reinforced brittle matrix composites. *ASCE Journal of Engineering Mechanics*, **118**, 2246–2264.

- Li, V.C. (1998). Engineered cementitious composites tailored composites through micromechanical modeling, in: N. Banthia, A. Bentur, A. Mufti (Eds.), *Fiber Reinforced Concrete: Present and the Future*, Canadian Society for Civil Engineering, pp. 64-97.
- Li, V.C. (2003) On engineered cementitious composites (ECC) A review of the material and its applications, *Journal of Advanced Concrete Technology*. 1 215-230.
- Lin, Z. and Li, V.C. (1997) Crack bridging in fiber reinforced cementitious composites with slip-hardening interfaces, *Journal of Mechanics and Physics of Solids* 45 763-787.
- Lin, Z., Kanda, T. and Li, V.C. (1999) On interface property characterization and performance of fiber reinforced cementitious composites, *Concrete Science and Engineering*. 1 173-184.
- Li, V.C. and Yang, E.H. (2007). Self healing in concrete materials. In: S. van der Zwaag (Ed.), *Self healing materials*, Springer, Dordrecht, pp. 161-193.
- Li, V.C., Mishra, D.K. and Wu, H.C. (1995). Matrix Design for Pseudo Strain-Hardening Fiber Reinforced Cementitious Composites. *RILEM Journal of Materials and Structures*, **28**, 586-595.
- Li, V.C., Wang, S. and Wu, C. (2001). Tensile Strain-hardening Behavior of PVA-ECC. *ACI Materials Journal*, **98**, 483-492.
- Marshall, D.B. and Cox, B.N. (1988). A J-integral method for calculating steady-state matrix cracking stresses in composites. *Mechanics of Materials*, **8**, 127–133.
- Mehta, P.K. and Gerwick, B.C. (1982). Cracking-corrosion interaction in concrete exposed to marine environment. *Concr. Int.*, **4** 45-51.
- Mehta P.K. and Monteiro P.J.M. (2006). *Concrete: Structure, Properties, and Materials*. Third Edition, McGraw Hill, New York.
- Meichsner, H. (1992). Autogenous Healing of Cracks in Concrete, *Beton und Stahlbetonbau*, (in German).

Mindess, S., Young, J.F. and Darwin, D. (2002). *Concrete*. 2nd Edition, Prentice Hall, 2002.

Moranville-Regourd, M. (1998). Cements Made From Blastfurnace Slag, *Lea's Chemistry of Cement and Concrete*, 4th Edition, P. C. Hewlett Ed., Arnold, London, pp. 663-674.

Misra, S., Yamamoto, A., and Tsutsumi, T. (1994). Application of Rapid Chloride Permeability Test to Qualify Control of Concrete. *Proc., Concrete Durability, 3rd Int. Conf.*, V. M. Malhotra, ed., 487-502.

Miyazato, S. and Hiraishi, Y. (2005). Transport properties and steel corrosion in ductile fiber reinforced cement composites. Proceedings of the Eleventh International Conference on Fracture, Turin, Italy, March, pp. 20-25.

Nancollas, G. H., and Reddy, M. M. (1971). Crystallization of Calcium Carbonate. *Journal of Colloid and Interface Science*, V.36 and 37, No. 3 and 4.

Neville, A. (2002). Autogenous healing - a concrete miracle?, *Concr. Int.* **24** 76-82.

Neville, A.M. (1996). *Properties of Concrete*. Fourth Edition, John Wiley & Sons, New York, pp. 884.

Ozbay, E., Sahmaran M., Lachemi M. and Yucel H.E. (2012). Self-healing of Microcracks in High Volume Fly Ash Incorporated Engineered Cementitious Composites. *ACI Materials Journal*, Accepted for Publication.

Perraton, D., Aitcin P.C. and Vezina D. (1988). Permeabilities of Silica Fume Concrete. *Permeability of Concrete ACI SP-108*, American Concrete Institute, Detroit, Michigan. pp. 63-84.

Powers, T.C. (1991). Structure and physical properties of hardened Portland cement paste. *Journal of American Ceramic Society*, Vol. 41 No 1. pp. 1-6.

Qian, S. and Li, V.C. (2008). Simplified inverse method for determining the tensile properties of strain hardening cementitious composites. *Journal of Advanced Concrete Technology*, **6**, 353-63.

Qian, S., Zhou, J., De Rooij, M.R., Schlangen, E. Ye, G., Van Breugel, K. (2009). Self-healing behavior of strain hardening cementitious composites incorporating local waste materials, *Cement and Concrete Composites*, **31** 613–621.

Reinhardt, H.W. and Jooss, M. (2003) Permeability and self-healing of cracked concrete as a function of temperature and crack width. *Cement and Concrete Research*, **33**, 981-985.

Reinhardt, H.W., Hearn, N., and Sosoro, M. (1997). Transport properties of concrete. *Penetration and Permeability of Concrete: RILEM Report 16*, Ed. H.W. Reinhardt. pp. 213-264.

Roy, D.M. (1992). The Effect of Blast Furnace Slag and Related Materials on the Hydration and Durability of Concrete. G. M. Idorn International Symposium, SP-131, J. Holm and M. Geiker, Eds., American Concrete Institute, Detroit, Michigan, pp. 195-208.

Sahmaran, M. and Li, V.C. (2007). De-icing salt scaling resistance of mechanically loaded Engineered Cementitious Composites. *Cement and Concrete Research*, **37**, 1035-1046.

Şahmaran, M. and Li, V.C. (2009a). Durability Properties of Micro-Cracked ECC Containing High Volumes Fly Ash. *Cement and Concrete Research*, **39**, 1033-1043.

Şahmaran, M., Yaman, İ. Ö. and Tokyay, M. (2007). Development of High Volume Low-Lime and High-Lime Fly-Ash-Incorporated Self Consolidating Concrete. *Magazine of Concrete Research*, **59**, 97-106.

Shi, C. (2007). Effect of mixing proportions of concrete on its electrical conductivity and the rapid chloride permeability test (ASTM C1202 or ASSHTO T277) results. *Journal of Cement and Concrete Research*, **34** (2004) 537-545.

Stang, H. and Li, V.C. (1999). *Extrusion of ECC-material*. In Proc. Of High Performance Fiber Reinforced Cement Composites 3 (HPFRCC 3) edited by H. Reinhardt and A. Naaman, Chapman & Hull, pp. 203-212.

Stark, J. and Ludwig, H.M. (1997b). Influence of Water Quality on the Frost Resistance of Concrete. *Freeze-Thaw Durability of Concrete*, J. Marchand, M. Pigeon, and M. Setzer Eds., E & FN Spon, London, pp. 157-164.

Sun, W., Zhang, Y.M., Yan, H.D. and Mu, R. (1999). Damage and damage resistance of high strength concrete under the action of load and freeze-thaw cycles. *Journal of Cement and Concrete Research*, **29** 1519–1523.

Suthiwarapirak, P., Matsumoto, T. and Kanda, T. (2002). Flexural fatigue failure characteristics of an Engineered Cementitious Composite and Polymer Cement Mortars. *Materials, Conc. Struc. Pavements*, **57**, 121-134.

Taylor, H.F.W. (1997). *Cement Chemistry, Second Edition*. Thomas Telford Publishing, London, pp. 459.

Ter Heide, N., (2005). Crack healing in hydrating concrete, TU Delft: MSc-thesis.

Wang, K., Jansen, D, Shah, S. and Karr, A. (1997). Permeability Study of Cracked Concrete. *Cement and Concrete Research*, Vol. 27 No. 3, pp. 381-393.

Wang, S. and Li, V.C. (2004). *Tailoring of pre-existing flaws in ECC matrix for saturated strain hardening*. Proceedings of FRAMCOS-5, Vail, Colorado, USA, pp. 1005–1012.

Wang, S. and Li, V.C. (2007). Engineered Cementitious Composites with high-volume fly ash. *ACI Materials Journal*, **104**, 233–241.

Weimann, M.B. and Li, V.C. (2003). Hygral behavior of engineered cementitious composites (ECC). *International Journal for Restoration of Buildings and Monuments*, **9**, 513-534.

Yang, E.H., Yang, Y. and Li, V.C. (2007). Use of high volumes of fly ash to improve ECC mechanical properties and material greenness. *ACI Materials Journal*, **104**, 620-628.

Yang, E., Şahmaran, M., Yang, Y. and Li, V.C. (2009). Rheological control in the production of Engineered Cementitious Composites. *ACI Materials Journal*, **106**(4) 357-366.

Yang, Y., Lepech, M.D. and Li, V.C. (2005). Self-healing of ECC under cyclic wetting and drying. Proceedings of Int'l Workshop on Durability of Reinforced Concrete under Combined Mechanical and Climatic Loads, Qingdao, China, 231-242.

Yang, Y., Lepech, M.D., Yang, E.H. and Li, V.C. (2009). Autogenous healing of engineered cementitious composites under wet-dry cycles. *Cement and Concrete Research*, **39**(5) 382-390.

Zhang, J. and Li, V.C. (2002). Monotonic and fatigue performance in bending of fiber reinforced Engineered Cementitious Composite in overlay system. *Cement and Concrete Research*, **32**, 415-423.

Zhou, J., Qian, S., Beltran, M.G.M., Ye, G., VanBreugel, K. and Li, V.C. (2009). Development of Engineered Cementitious Composites with Limestone Powder and Blast Furnance Slag. *Rilem Journal of Materials and Structures*, **43**, 803-814.